Tissue Eng Regen Med (2023) 20(4):563–580
https://doi.org/10.1007/s13770-023-00539-8

Online ISSN 2212-5469 TERM

REVIEW ARTICLE

Acoustic and Magnetic Stimuli-Based Three-Dimensional Cell Culture Platform for Tissue Engineering

Ju Yeon Seo[1,5] · Song Bin Park[2] · Seo Yeon Kim[1] · Gyeong Jin Seo[1] · Hyeon-Ki Jang[3] · Tae-Jin Lee[1,4]

Received: 22 December 2022 / Revised: 16 February 2023 / Accepted: 15 March 2023 / Published online: 13 April 2023

Abstract In a conventional two-dimensional (2D) culture method, cells are attached to the bottom of the culture dish and grow into a monolayer. These 2D culture methods are easy to handle, cost-effective, reproducible, and adaptable to growing many different types of cells. However, monolayer 2D cell culture conditions are far from those of natural tissue, indicating the need for a three-dimensional (3D) culture system. Various methods, such as hanging drop, scaffolds, hydrogels, microfluid systems, and bioreactor systems, have been utilized for 3D cell culture. Recently, external physical stimulation-based 3D cell culture platforms, such as acoustic and magnetic forces, were introduced. Acoustic waves can establish acoustic radiation force, which can induce suspended objects to gather in the pressure node region and aggregate to form clusters. Magnetic targeting consists of two components, a magnetically responsive carrier and a magnetic field gradient source. In a magnetic-based 3D cell culture platform, cells are aggregated by changing the magnetic force. Magnetic fields can manipulate cells through two different methods: positive magnetophoresis and negative magnetophoresis. Positive magnetophoresis is a way of imparting magnetic properties to cells by labeling them with magnetic nanoparticles. Negative magnetophoresis is a label-free principle-based method. 3D cell structures, such as spheroids, 3D network structures, and cell sheets, have been successfully fabricated using this acoustic and magnetic stimuli-based 3D cell culture platform. Additionally, fabricated 3D cell structures showed enhanced cell behavior, such as differentiation potential and tissue regeneration. Therefore, physical stimuli-based 3D cell culture platforms could be promising tools for tissue engineering.

Keywords 3D cell culture · Acoustic · Cell aggregate · Magnetic force · Tissue engineering

✉ Tae-Jin Lee
leetj@kangwon.ac.kr

[1] Division of Biomedical Convergence, Department of Medical Biotechnology, College of Biomedical Science, Kangwon National University, Chuncheon-si, Gangwon-do 24341, Republic of Korea

[2] Department of Bio-Health Technology, College of Biomedical Science, Kangwon National University, Chuncheon-si, Gangwon-do 24341, Republic of Korea

[3] Division of Chemical Engineering and Bioengineering, College of Art Culture and Engineering, Kangwon National University, Chuncheon-si, Gangwon-do 24341, Republic of Korea

[4] Department of Bio-Health Convergence, Kangwon National University, Chuncheon-si, Gangwon-do 24341, Republic of Korea

[5] Department of Biomedical Science, Kangwon National University, Chuncheon-si, Gangwon-do 24341, Republic of Korea

1 Introduction

In a conventional two-dimensional (2D) culture method, cells are attached to the bottom of a culture dish, such as artificial plastic or glass substrate, to grow into a monolayer [1–3]. This 2D culture method is easy to handle, cost-effective, reproducible, adaptable to growing many different types of cells, and could reduce the use of animal models [1, 4]. However, monolayer 2D cell culture conditions are far from those of natural tissue [3–5].

In 2D cell culture, cells grow only in a monolayer and cannot pile up, as do all natural cells [3]. For 2D cell culture, cells are isolated from tissue, and the diverse morphology of the cells is changed or lost [3, 6, 7]. The change in cell morphology affects cellular function [8, 9], the organization of the structure within the cell [3], and cell

secretion and signaling [10, 11]. Studies showed that interactions between cells and the external environment were interrupted, and cells lost their polarity, that changing the cellular response to various phenomena such as apoptotic signals [12–14]. Receptor expression [3], oncogene expression [3], interaction with the extracellular matrix (including the basement membrane) [3], and overall architecture were also affected [3]. For example, tumor tissue is surrounded by a tumor microenvironment that consists of several different types of cells, matrix components, and signal molecules *in vivo* [15]. Cancer microenvironment components, such as vascular structure, acidic conditions, hypoxic regions, and tumor and stromal cell interactions, modulate the response to anticancer drugs [16]. However, 2D cell cultures with tumor cells cannot reproduce these complex conditions. Therefore, tumor cells grown in 2D culture showed a 95% drug failure rate, and 2D culture systems could not be utilized as reliable predictors of *in vivo* drug efficacy and toxicity or as a drug development model [17, 18]. As a result, the need for a three-dimensional (3D) culture system was highlighted [3–5].

Cells grown in 3D cell culture methods showed improvements in basic biological cell mechanisms, including, viability, morphology, proliferation, differentiation, cell–cell communication, drug metabolism, gene expression, protein synthesis, and *in vivo* relevance compared to 2D cell culture [3, 19]. For example, in 2D cultured cells, polarized and binding proteins are concentrated on the surface where the cells attach to the culture plate, but receptors and adhesion molecules in 3D cultured cells are more evenly and naturally spread on the cell surface [20]. And cells grown in a 3D culture system formed more tissue-like structures caused by the homogeneous expression of adhesion molecules distributed on the cell surface [21]. In oxidative stress (caused by hydrogen peroxide) and potentially toxic heavy metal (silver) treatment, 3D cultured skin cells were more viable compared to 2D cultured cells [22]. Interestingly, genetic analysis of human tissues, 3D cultured cancer cell, and animal tumor moder showed that human tissues and 3D cell cultures had greater correlation in profile compared to animal models [23, 24]. Therefore, 3D cell cultures have been widely used in cancer research, stem cell research, drug discovery, and disease research [25].

3D cell culture methods include hanging drop, scaffolds, hydrogels, cell sheets (CSs), microfluid systems, and bioreactor systems [26–31]. Recently, external physical stimulation-based 3D cell culture platforms, such as acoustic and magnetic forces, were introduced. In this article, we will review acoustic and magnetic-based 3D cell culture platforms, especially their use in tissue engineering.

2 Acoustic-based 3D cell culture platform

An acoustic wave is a kind of mechanical wave [32], and frequencies from kilohertz-to-megahertz are easily generated [33, 34]. Acoustic waves can be divided into bulk acoustic waves (BAWs) and surface acoustic waves (SAWs), according to the method of generation [35, 36]. Acoustic waves are usually generated by applying an alternating voltage to piezoelectric materials [35, 37, 38]. BAWs are generated via piezoelectric transducers, which can convert electrical signals into mechanical waves [35]. Acoustic waves reflected from a reflector can form standing waves containing pressure nodes and pressure antinodes [35]. The number of standing waves can be adjusted by controlling the acoustic wave frequency [39]. SAWs are generated by interdigitated transducers patterned on a piezoelectric surface [40]. Interdigitated transducers are mostly used in pairs. Two or four interdigitated transducers can be used to generate one-dimensional or 2D wave interference patterns [40, 41].

Acoustic waves can establish pressure distributions in fluids [35]. This produces an acoustic radiation force (ARF) due to an acoustic field gradient [42]. Objects in a strong-gradient acoustic field can be manipulated using [32]. ARF can induce suspended objects to gather in the pressure node (or pressure antinode) region [42]. After that, objects are no longer randomly distributed but are concentrated in nodal planes [43]. Objects gathered on the nodal plane can aggregate to form clusters. Bjerknes force is generated between objects vibrating in close range that can help clusters remain stable and close together [44]. This is called an "acoustic trap," and BAWs and SAWs can form acoustic traps [44, 45].

Acoustic technology using acoustic waves has contactless, label-free, excellent biocompatibility, and flexibility properties. It can manipulate cells while maintaining cell-specific conditions, which is a promising technology for fabricating 3D spheroids [37, 41, 46]. Below, we introduce several acoustic-based 3D cell culture platform systems and their applications for tissue engineering.

2.1 Spheroid formation with acoustic-based 3D cell culture platform

The ability to manipulate cells using acoustic waves can also be applied to 3D cell culture. Jeger-Madiot et al. demonstrated the use of acoustic levitation technology to form a stem cell spheroid [47]. They designed a 3D cell culture device containing a polydimethylsiloxane (PDMS) frame with a microscope cover glass and a 2 MHz ultrasonic transducer (Fig. 1A). PDMS has excellent biocompatibility and gas permeability and is commonly used in

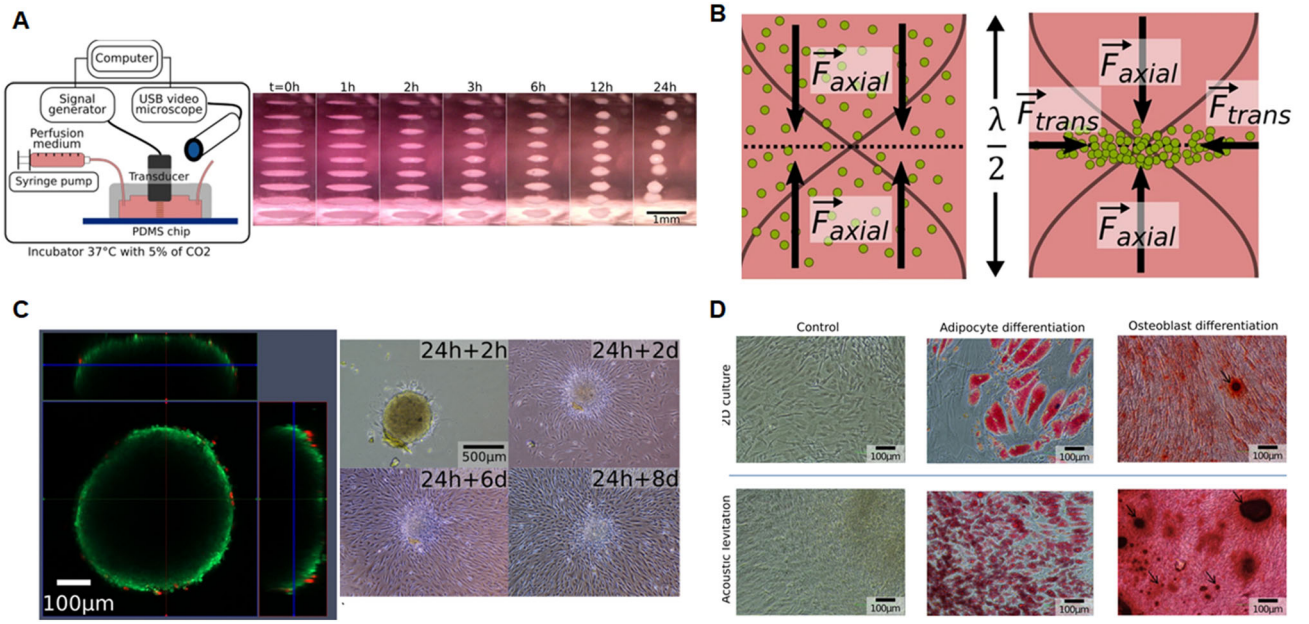

Fig. 1 Spheroid production using acoustic levitation techniques. **A** Design and process of the device used in the experiment for spheroid formation. A computer sends a signal that induces wave formation, and a transducer converts this electrical energy into acoustic energy for acoustic levitation. Cells aggregated in a sheet then form and exhibited a spherical shape after the passage of time. **B** Schematic diagram showing the principle of CS formation in the device and actual experiment using particles. Acoustic radiation force (ARF) was generated by acoustic energy. **C** Confocal and fluorescence images of a spheroid surface generated in an acoustic levitation device (left panel). Phase-contrast image of a spheroid re-seeded into a culture dish (right panel). The ability of spheroids to reattach to the dish was observed for 8 days. **D** Images of MSCs differentiated into adipocytes and osteocytes. Adipocyte differentiation was confirmed using Oil red O staining, and osteocyte differentiation was confirmed using alizarin red staining. MSCs cultured under levitation conditions had more adipocytes and osteoblast nodules than 2D-cultured cells. "Self-organization and culture of mesenchymal stem cell spheroids in acoustic levitation" by Jeger-Madiot et al. is licensed and used under CC BY 4.0. Excerpt from original

cell culture and tissue engineering [48]. An ultrasonic transducer can produce sine waveform acoustic waves with a frequency of 2.15 MHz. Microscope cover glass acts as an acoustic reflector. Mesenchymal stem cells (MSCs) were injected into a 3D cultured device and cultured for 24 h. MSCs self-assembled and formed spheroids after 10 h (Fig. 1A). After the cells were located in the nodal plane of the acoustic wave, they were aggregated by ARF transverse waves (Figs. 1A, 1B). After 24 h, the generated spheroids showed high viability and high reattachment levels when re-seeded to a culture dish, indicating that MSC spheroids maintained the ability to re-adhere to a culture dish (Fig. 1C). In osteogenic and adipogenic differentiation, 3D-cultured MSC spheroids formed in acoustic pressure showed enhanced osteogenic and adipogenic differentiation compared to 2D-cultured cells, indicating that levitation-induced physical effects enhanced osteogenic and adipogenic differentiation [47] (Fig. 1D).

A previous 2D cell culture study showed that physical stimulation could up-regulate the expression levels of mechanoresponsive genes and cell proteins. Among mechanoresponsive genes and proteins, pressure-induced mechanosensitive gene and protein (PIEZO 1/2) is known to regulate functions such as differentiation and cytoskeletal restoration in 2D cultured stem cells [48–52]. However, PIEZO 1/2 expression in 3D cultured stem cells has not been investigated yet. Im et al. investigated the cellular mechanisms of 3D cultured stem cells related to the expression of PIEZO1/2 and developed a new sub-aqueous free-standing (FS) 3D cell culture device that includes a piezoelectric actuator and a reflector to create 3D cell aggregates (Fig. 2A) [53]. The piezoelectric actuator was installed at the bottom of the device, and the reflector was installed at the top. In addition, the piezoelectric actuator had a 1.6 MHz resonance frequency to generate an acoustic standing wave. After human adipose-derived stem cells (hADSCs) were injected into the device, the cells moved quickly to the node regions of the wave and aggregated within 30 min (Fig. 2B). Cell aggregates generated using acoustic pressure are called "pressuroids." The cellular properties of pressuroids were compared to those of cell aggregates formed by hanging drop (HD) and the forced-floating method (FFM), common 3D cell culture methods. PIEZO2 expression in pressuroids was higher than that of cells in the HD and FFM groups. Enhanced PIEZO2 expression led to the improved expression of PI3K, VEGF, CCND1, and PCNA (Fig. 2C). CCND1 and PCNA activate cell proliferation [54, 55] and PI3K and

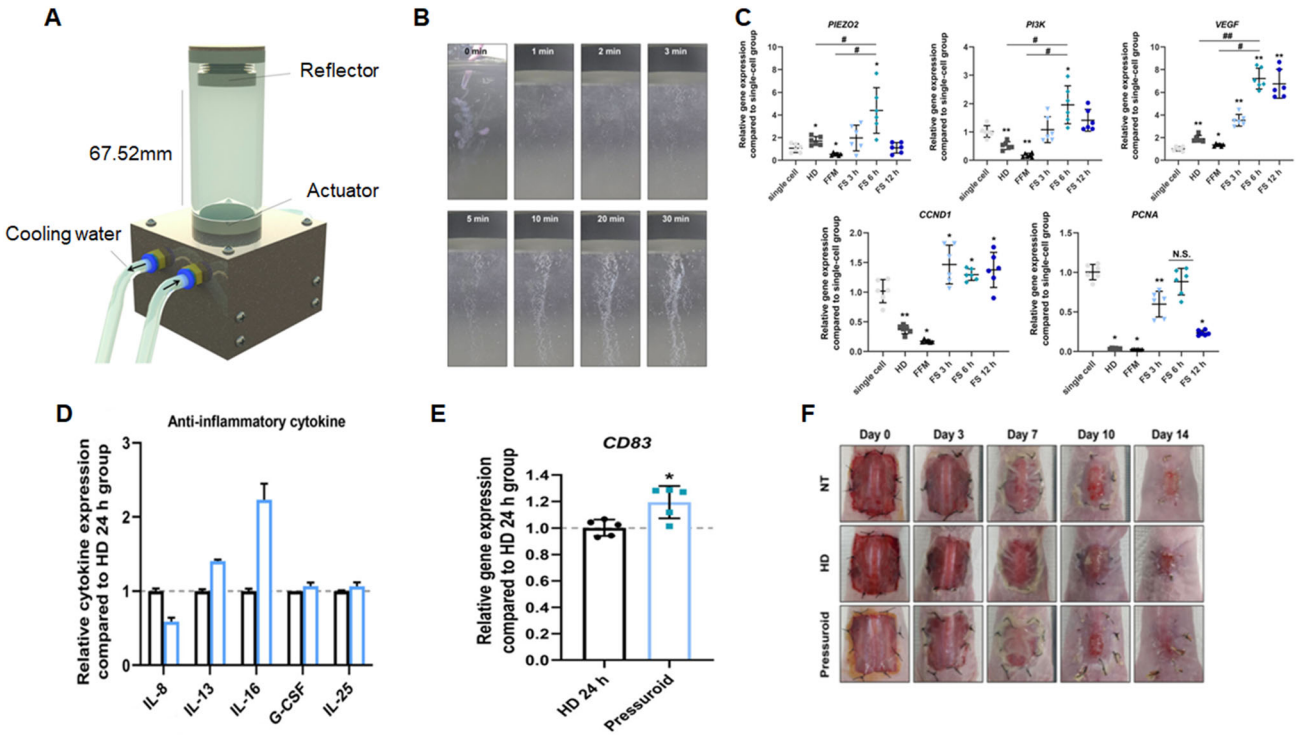

Fig. 2 Investigation of gene expression and application of pressuroids (3D cell aggregates) generated from free-standing (FS) devices to *in vivo* experiments. **A** Schematic diagram of the FS device. **B** Image showing that cells were aggregated over time after hADSCs were injected into the device. **C** PIEZO2, PI3K, VEGF, CCND1, and PCNA gene expression in single cells, hanging drop (HD) group, forced floating (FFM) group, and FS group (pressuroid). **D**, **E** Gene expression of anti-inflammatory cytokines and M2 macrophage marker CD38. The blue box is pressuroids, and the black box is the HD group cultured for 24 h. The HD group served as the control. **F** Images of wounds on a skin wound model on days 0, 3, 7, 10, and 14 after HD and pressuroid treatment. "Subaqueous free-standing 3D cell culture system for ultrafast cell compaction, mechano-inductive immune control, and improving therapeutic angiogenesis" by Im et al. is licensed and used under CC BY. Excerpt from original

VEGF play important roles in angiogenesis [56]. The expression levels of anti-inflammatory cytokines were also improved in pressuroids compared to HD cells (Fig. 2D). Additionally, CD38, an M2 macrophage phenotype marker, was increased in pressuroids (Fig. 2E). To analyze wound healing efficacy, pressuroids were transplanted into mouse skin wounds. The pressuroids showed enhanced skin regenerative capabilities compared to HD cells (Fig. 2E) [53]. Anti-inflammatory cytokines secreted from pressuroids induced macrophages into the M2 type [57]. M2 macrophages promoted epithelization to influence wound treatment [58]. These results indicate that acoustic pressure could form spheroids and activate mechanoresponsive genes/proteins, thus promoting angiogenesis and epithelization in skin wounds.

2.2 Cell fiber formation with acoustic-based 3D cell culture platform

Ultrasonic waves have been used to manipulate suspended particles. A standing wave ultrasound field applied to a suspension moved particles to the minimum acoustic pressure area, where particles were held, creating a predictable heterogeneous distribution [59]. Koo et al. demonstrated the formation of 3D fibroblast networks using an acoustic wave [60]. 3D network-structured tissue is needed in engineered organ and drug development [60]. For example, 3D microvascular networks are important and promising network-structured tissue and essential for treating ischemic tissues in clinical applications [61, 62]. A necrotic core formed within engineered tissue due to limited oxygen and nutrient supply, and the cells were located close to a blood capillary network [63–65]. Koo et al. designed a 400 μm square-shaped glass capillary. The glass capillary was then glued to two ultrasound transducers. One was a 0.5 mm thick 10 × 10 mm ultrasound transducer for 4 MHz actuation, and the other was a 1 mm thick, 10 × 10 mm ultrasound transducer for 2 MHz actuation (Fig. 3A). To generate 3D fibroblast networks, fibroblasts were mixed with alginate. The glass capillary was then perfused with acoustic focusing. After acoustic focusing, fibroblasts containing alginate hydrogel were

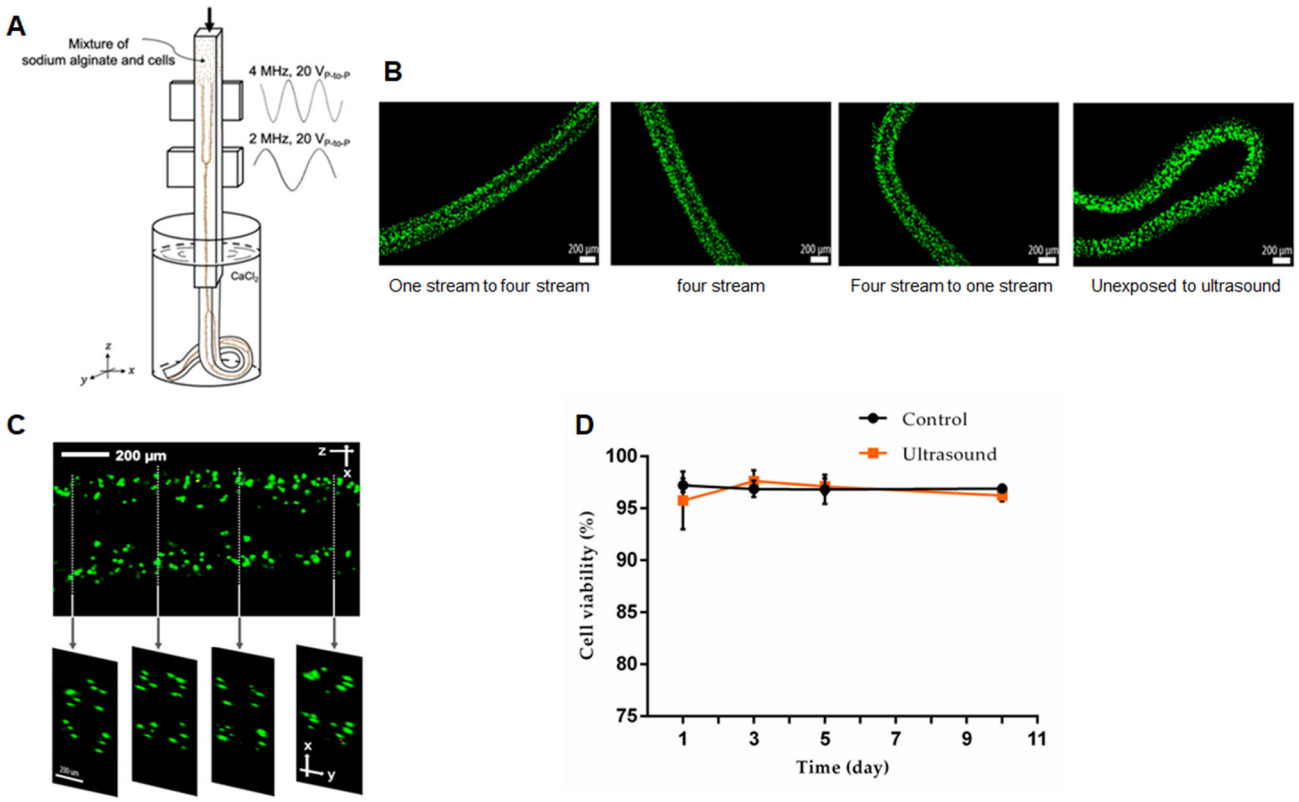

Fig. 3 Ultrasound-modulated fibroblast stream in an alginate hydrogel. **A** Conceptual sketch of the network generator. **B** Images of fibroblast cells manipulated with ultrasound. **C** Confocal microscopy image of aligned fibroblast cells in four streams. **D** Viability of ultrasound exposed or unexposed fibroblasts. "Acoustic cell patterning in hydrogel for three-dimensional cell network formation" by Koo et al. is licensed and used under CC BY. Excerpt from original

injected into a $CaCl_2$ solution for gelation. When ultrasound at a frequency of 2 MHz was used to treat the fibroblasts within the hydrogel, one stream of fibroblasts was formed. The frequency was then changed from 2 to 4 MHz. One stream of fibroblasts was converted to four streams of fibroblasts within the hydrogel (Figs. 3B, 3C). In contrast, ultrasound-untreated fibroblasts were distributed within the gel (Fig. 3B). A live/dead cell assay found that ultrasound was not cytotoxic to fibroblasts until 10 days (Fig. 3D) [60]. This study showed that the acoustic cell patterning method had the potential for forming living cell 3D networks within the hydrogel.

Ultrasound standing waves could be used to construct myocellular populations for engineering aligned muscle tissue structures (Fig. 4A) [66]. Armstrong et al. fabricated an acrylic plate with a cavity for suspending cells contained in a petri dish [66]. This cavity was flanked by four lead zirconate titanate piezo transducers to induce a cell pattern (Fig. 4B). To analyze acoustic patterning compatibility, myoblasts suspended in cell medium were exposed to a 2.0–2.1 MHz field for 30 min. The ultrasound did not affect cell metabolic activity, cell proliferation, myogenic gene expression, or muscle protein expression. For muscle tissue engineering, ultrasound standing waves (2.0–2.1 MHz) were applied to myoblast-seeded collagen hydrogel for 30 min. Cell fiber with a width of 60–80 μm, mimicking native tissue, was formed by ultrasound treatment. After gelation, the patterned hydrogel was removed from the ultrasound field and cultured for one day, and differentiated with a myogenic medium for muscle tissue. Cell morphology changed from a round shape to adherent myoblasts (Fig. 4C). The myoblast-patterned composition was maintained over time (Fig. 4C). Next, mechanical anisotropy was analyzed parallel or orthogonal to the patterned cell line with quasi-static tensile. Young's modulus for parallel configuration was increased by 80% compared to an orthogonal setup (Fig. 4D). The authors repeated this experiment with gelatin methacryloyl hydrogel. Acoustic-patterned myoblasts in gelatin methacryloyl hydrogel showed enhanced myofibrillogenesis, which is the formation of muscle fibers. These results indicate that acoustic treatment could form patterned cells and engineered cell fibers.

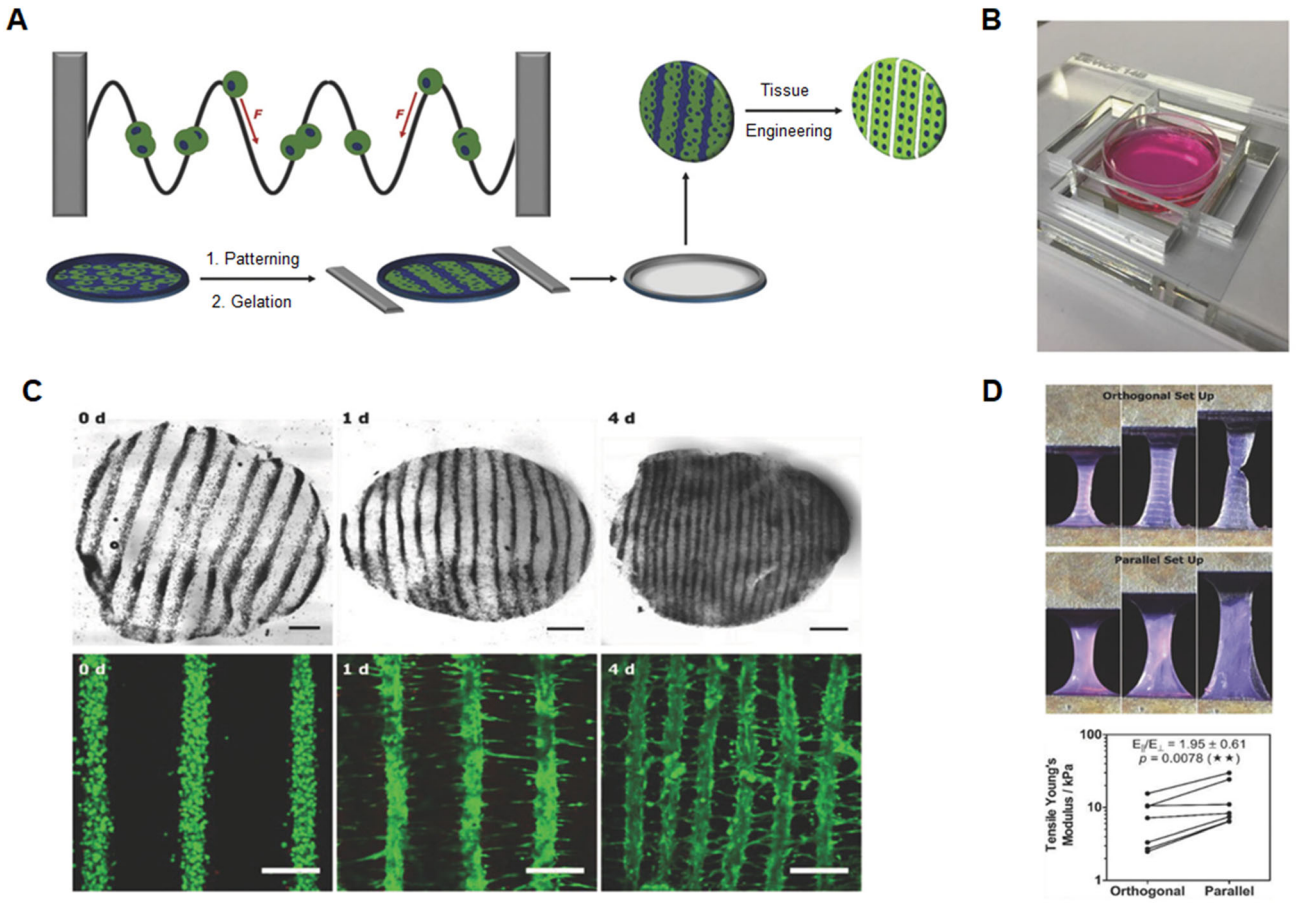

Fig. 4 Engineering pattern muscles using collagen. **A** Scheme of engineering anisotropic muscle tissue using acoustic cell patterning. **B** Images of the acoustic patterning device. Two pairs of piezo transducers were used to generate ultrasonic standing waves across a petri dish of cells. **C** Bright-field and confocal fluorescence images of acoustic pattern myoblasts in 3 mg mL^{-1} collagen. 4 mm diameter biopsy cross-section separated over 4 d was stained with calcein (green, viable cell) and ethidium homodimer (red, nonviable cell). Bright-field scale bar, 0.5 mm. Fluorescence scale bar, 200 µm. D Images of mechanical testing with cell lines (top) and tensile Young's modulus for the orthogonal and parallel configurations (bottom). Testing was applied either orthogonal or parallel to the cell lines. Paired data from seven separate tissues (one-tailed Wilcoxon matched pairs test); $^{**}p \leq 0.01$. "Engineering anisotropic muscle tissue using acoustic cell patterning" by Armstrong et al. is licensed and used under CC BY. Excerpt from original

2.3 Vascular network formation with acoustic-based 3D cell culture platform

An acoustic-based 3D cell culture platform has been applied to form a vascular network. Garvin et al. [67] developed ultrasound standing wave field (USWF) technology to form vascularized 3D collagen-based hydrogel with human endothelial cells. To treat cells with USWF, a plastic exposure tank was prepared and filled with degassed, deionized water at room temperature. The acoustic source was a 1 MHz unfocused transducer formed by a 2.5-cm diameter piezoceramic disk [68]. This transducer was located at the bottom of the water tank. Samples were loaded onto cell culture plates with a silicone elastomer bottom. The plates were affixed to a three-axis positioner to allow precise control over their location in the sound field within the tank [67]. Human umbilical vein endothelial cells (HUVECs) in collagen solution were injected onto the culture plate and then exposed to USWF. USWF induced planar bands of endothelial cells in collagen gel. The collagen solution was polymerized during the USWF treatment period. Polymerization preserved the band pattern of endothelial cells after USWF removal. Cell bands were separated at half-wavelength distance for a 1 MHz (750 µm). Additionally, endothelial cells treated with USWF formed anastomosing networks. The effects of various USWF exposure parameters on the initial spatial pattern of endothelial cells within collagen hydrogels were also analyzed [69]. Endothelial cells in collagen gel were treated with two acoustic sources, 1 MHz and 2 MHz. The pattern of endothelial cells was changed by USWF [69]. When endothelial cells in collagen were exposed to

1 MHz, planar bands of cells were observed at pressure amplitudes of 0.1 MPa, and the distance between bands was 750 μm [69]. When cells in collagen gel were exposed to 2 MHz, planar cell bands were observed at pressure amplitudes of 0.08 MPa, and the distance between cell bands was 375 μm [69]. This study demonstrated that USFW could generate vascular networks with endothelial cells in collagen gel and that their spatial patterning could be controlled by the frequency [69]. Consequently, ultrasound-induced spatial patterning of endothelial cells could directly affect the shape of vascular networks.

Multiple transducers and alternative-source geometry allow cells of different spatial patterns to be generated throughout 3D-engineered tissues [70]. Hu et al. performed digital acoustic 3D cell assembly within photo-crosslinked methacrylate gelatin hydrogel sheets [70]. Six digitally controlled waves from interdigital transducers (IDTs) provided a high degree of freedom (wave vector combination, frequency, phase, and amplitude) that enabled versatile biomimetic microcell patterning in hydrogel sheets. IDTs were made from a lithium niobate substrate that showed six-fold symmetry with electromechanical coupling coefficient and sound speed. These IDTs generated uniform surface acoustic waves over a wide range of frequencies that could obtain a uniform acoustic potential structure in the hydrogel layer. The acoustic device was controlled by a cell phone. Through this six-beam-based system, more complex wave vectors and phase relations could be formed compared to traditional acoustic systems. Various biomimetic patterns were formed on each CS by six symmetric wave vector modulations, including functional repeating unit of liver which was hexagonal shaped lobules, a vessel-like tube, and a honeycomb grid within the hydrogel sheet. HUVECs and vascular smooth muscle cells (SMCs) were used to form an *in vitro* vessel construct. In the 3D view, HUVECs were wrapped inside SMC layers. The fabricated 3D vessel construct was transferred to a culture dish for long-term culture. After 5 days of culture, HUVECs and SMCs proliferated, and cell density in the vessel wall increased. Overall, this digital acoustic 3D cell assembly system could fabricate complex cellular constructs, including vessel networks. Therefore, this digital acoustic 3D cellular construct manufacturing system might have potential applications in tissue engineering.

3 Magnetic-based 3D cell culture platform

Magnetic targeting consists of two components [71]. One is a magnetically responsive carrier, which works by superparamagnetism, where objects are strongly magnetized under a magnetic field and have no remnant or residual magnetization without the magnetic field? [71]. The other is a magnetic field gradient source, such as a magnetic force, that could attract or position magnetic-responsive carriers in organs or tissues [71]. A magnetic field can be generated by the permanent magnets of magnetic bioreactors to produce an oscillating pulse [71]. In magnetic-based 3D cell culture platforms, cells were aggregated by changing the magnetic force [72]. Magnetic fields (called magnetophoresis) can manipulate cells by two different methods: positive magnetophoresis and negative magnetophoresis. Positive magnetophoresis is a way of imparting magnetic properties to cells by labeling them with magnetic nanoparticles (MNPs) [73]. The direct endocytosis of MNPs by cells can induce magnetic sensitivity [74, 75]. MNPs induced cytotoxicity when they were introduced into cells by endocytosis [76]. Several methods have been useful in avoiding cytotoxicity. Using magnetoferritin instead of iron oxide MNPs increased cell viability [77]. Magnetoferritin is a biological MNP made by synthesizing ferritin, an iron storage protein, and iron oxide MNPs [78]. It has low toxicity and high biocompatibility [79, 80]. Another approach is cell surface engineering, where polymerized MNPs are deposited on the cell membrane without permeating the cytoplasm [81]. Thus, cells with magnetic properties could be levitated by an external magnetic force [82]. Positive magnetophoresis could be used to assemble cells to form 3D structures, such as spheroids [77, 83] and CSs [84, 85]. It is a useful tool in platforms for 3D cell culture [73].

Negative magnetophoresis, like positive magnetophoresis, can be a useful technique for assembling cells in three dimensions by levitation [73]. Negative magnetophoresis is a label-free principle-based method that does not label MNPs to cells. It eliminates MNP problems such as cytotoxicity [73]. In this method, cells are contained within a paramagnetic salt solution [86] or ferrofluid [87]. Manganese (II) chloride ($MnCl_2$) [88, 89], gadolinium (III) chloride ($GdCl_3$) [89, 90], or Gd(DTPA) [90, 91] are widely used as paramagnetic salt solutions. They are readily available, relatively inexpensive, and offer the advantage of providing a transparent property for making samples observable [89, 92]. A ferrofluid was developed as a stable magnetic colloid liquid with magnetic properties by the incorporation of magnetic particles [87, 93]. Its magnetic susceptibilities could be controlled by adjusting its concentration, thereby imparting higher magnetic susceptibilities than paramagnetic salt solution [92]. However, due to its opaque property, fluorescent staining was required to observe the sample [94]. Cells with diamagnetic properties exhibited less magnetization than paramagnetic salt solution or ferrofluid, thereby focusing on lower magnetic field regions within the magnetic field [94].

Magnetic-based techniques offer several advantages, including minimal impact on viability, simple and low-cost

design, and low sensitivity to environmental parameters, such as ion concentrations and pH [95]. Here, we introduce a magnetic-based 3D cell culture platform.

3.1 CS formation with magnetic based 3D cell culture platform

Upon *in vivo* transplantation, tissues produced by CS engineering can adhere to the host's surface without separate suturing. They can also form dense cell-like structures [96], enabling the maintenance of cell–cell interactions for tissue regeneration [97]. CS engineering has been applied to various tissues, such as the heart, bones, bladder, cornea, esophagus, and liver [98], with some successful clinical outcomes [99]. To develop a thick-layered 3D cell structure for bone tissue engineering (TE) purposes, Silva et al. proposed a magnetic-responsive heterotypic CS fabrication (ADSCs/HUVECs/ADSCs) technique called magnetic force-based TE (Mag-TE) [100]. High levels of hierarchically organized bone tissue, such as vascularization, were difficult to reproduce. Therefore, CSs for bone regeneration remains at the initial stages [99, 101, 102]. Successful replacement of engineered bone tissue to defects was depended on rapid and sufficient vascularization in the engineered bone tissue which needed for optimal cell survival and integration to the tissue *in vivo* [103]. Magnetic-responsive heterotypic CSs enable a thick cellular multilayer structure. First, magnetite Fe_3O_4 nanoparticles (MNPs) were synthesized by the co-precipitation reaction of ferrous and ferric salts. To form heterotypic magnetic CSs, MNPs were delivered to ADSCs for four hours. MNP-treated ADSCs were then detached and transferred to an ultra-low-attachment culture plate. To provide a magnetic force, commercial neodymium rod magnets were left at the bottom of the reverse side of the culture plate during culture. Twenty-four hours after ADSC plating, HUVECs magnetically labeled by MNPS were seeded onto the previously fabricated ADSC monolayer. Twenty-four hours after HUVEC plating, magnetically labeled ADSCs were seeded once again. Through this procedure, magnetically labeled ADSCs and HUVECs were successfully organized in a triple sheet with HUVECs between two sheets of ADSCs (ADSCs/HUVECs/ADSCs). In osteogenic differentiation with osteogenic differentiation medium, heterotypic CSs showed increased alkaline phosphatase (ALP) activity, matrix mineralization, osteopontin, and osteocalcin. Interestingly, heterotypic CSs caused osteogenesis without an osteogenic differentiation medium. Finally, *in vivo* angiogenic potential was analyzed using a chick chorioallantoic membrane (CAM) assay. The results showed that endothelialized CSs recruited new vessels to an extent similar to basic fibroblast growth factor (bFGF), and CSs were incorporated into the host tissue. Thus, magnetic forces showed remarkable outcomes in the fabrication of CSs. Heterotypic CSs has been shown to be effective in stimulating *in vitro* osteogenesis. Furthermore, heterotypic CSs enhanced angiogenesis in *in vivo*. Therefore, this magnetic-based heterotypic CS fabrication system could be useful in tissue engineering.

Another study on magnetic-based CS formation was conducted by Koto et al. [104]. They fabricated CS using dental epithelial cells (DECs) and dental mesenchymal cells (DMCs) (CC sheets) using magnetic force [104]. In tooth and periodontal tissue regeneration, attempts to regenerate dentin, periodontal ligaments, and alveolar bone have not been successful because dental enamel (DE) regeneration, with its specific developmental process, remains difficult [105, 106]. The formation and maturation of DE are induced by epithelial-mesenchymal interaction, which depends on the relationship between DECs and DMCs [105, 107]. Therefore, Koto et al. fabricated CC sheets with DECs and DMCs by Mag-TE [104]. They obtained MNPs from Nano3D Biosciences and delivered them to DECs and DMCs isolated from the third molar tooth buds of 6-month-old porcine lower jaws [104]. For cytotoxicity assay, MNPs were treated with DECs and DMCs at various concentrations (0, 50, 100, 150, or 300 pg magnetite/cell) [104], and there was no significant change in the absorbance in DECs and DMCs at any concentration (Fig. 5A). To form CC sheets, DECs and DMCs were treated with MNPs (100 pg magnetite/cell) for 6 h. Then, MNP-labelled DMCs were seeded onto 24-well ultra-low attachment cell culture plates, and cylindrical neodymium was placed on the reverse side of the ultra-low-attachment plate for 24 h. Then, MNC-labelled DECs were seeded onto the same culture plate and cultured another 24 h with neodymium. Then, neodymium was removed from the plate. Optical observations showed that CC sheets with multilayered structures were successfully constructed (Fig. 5B). MNPs were distributed over the CC sheet, as confirmed by iron staining (Fig. 5B). And the mRNA expression of AMEL, ENAM, AMBN, Runt-related transcription factor 2 (RUNX2), collagen Iα2 (COL1α2), dentin sialophosphoprotein (DSPP), and collagen IV 1 (COL4 1) in the CC sheet was analyzed (Fig. 5C). Compared to the mixed DEC and DMC sheet, AMEL, ENAM, AMBN, RUNX2, COL1α2, and COL4 1 mRNA expression was up-regulated and COL1α2 and DSPP were not significantly different (Fig. 5C). AMEL, ENAM, and AMBN are known as differentiation markers of DECs that differentiate into ameloblasts [108–113]. Finally, in immunofluorescence staining, COL4, which is expressed in the basement membrane of presecretory and late mature-stage tooth germs, was expressed in the middle region of the CC sheet (Fig. 5D). Therefore, these results indicated that DEC and DMC multilayered CS was successfully

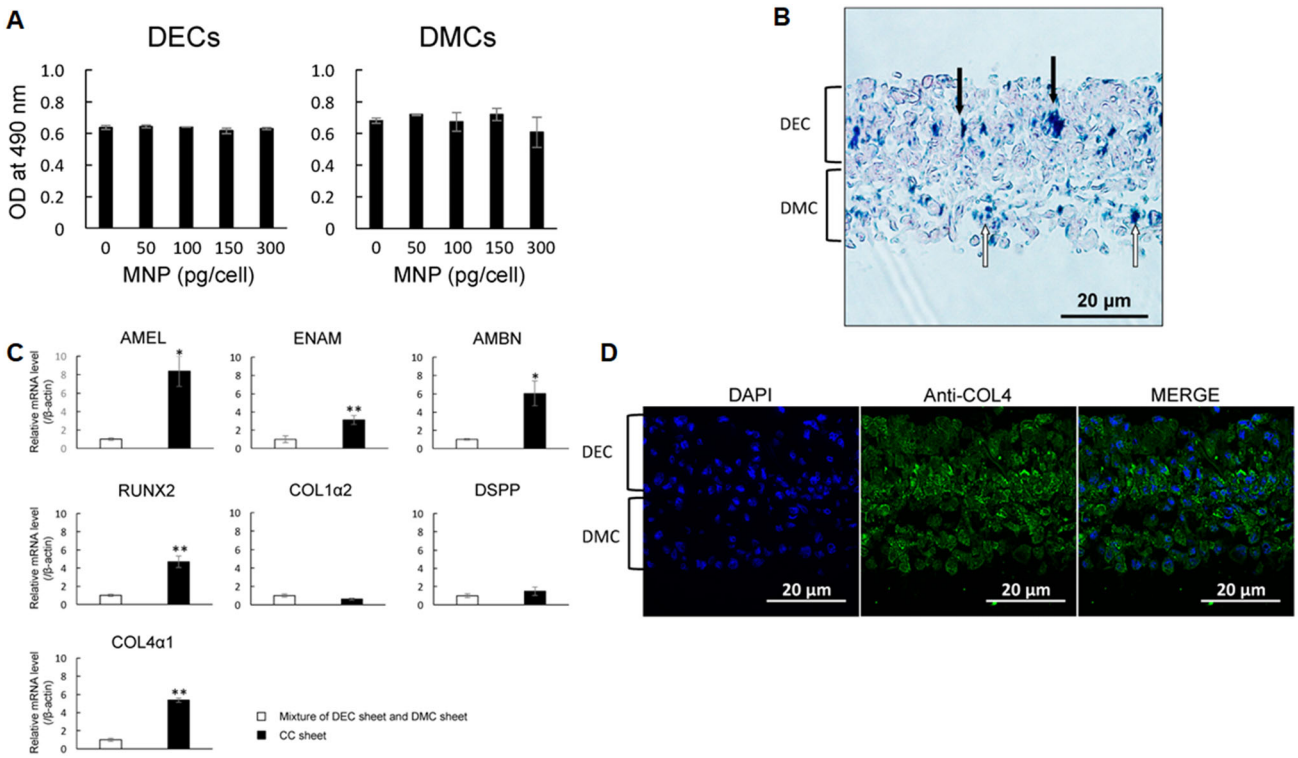

Fig. 5 Cell sheet formation with dental epithelial cells and dental mesenchymal cells by magnetic nanotechnology. **A** Cytotoxic effect of MNPs on dental epithelial cells (DECs) and dental mesenchymal cells (DMCs) assessed by MTS assays. MNPs at 0, 50, 100, 150, or 300 pg magnetite/cell were added to the cells at confluency. After the cells were maintained for 24 h in the presence or absence of MNPs, the MTS assay was performed; $p > 0.05$, ANOVA. **B** Microscopic observation of a CC sheet after iron staining (× 200). The filled arrows indicate MNPs in the DEC layer. The white arrows indicate MNPs in the DMC layer. Scale bar = 20 μm. **C** mRNA expression levels of AMEL, ENAM, AMBN, RUNX2, COL1α2, DSPP, and COL4α1 in the CC sheet analyzed by real-time RT-PCR. A mixture of DEC and DMC sheets prepared separately was used as the control. Real-time RT-PCR data were normalized to the expression levels of β-actin mRNA. Independent experiments were repeated twice. The data represent the mean ± SD of triplicate samples; * $p < 0.05$, ** $p < 0.01$. **D** Fluorescence microscopy observation of a CC sheet (× 200). 4,6 diamidino-2-phenylindole (DAPI) (blue) was used to stain the nuclei (left). COL4 was stained with a specific antibody. COL4-expressing cells (green) were identified around the border of the DEC and DMC layers (middle, right). Scale bars = 20 μm. "Porcine dental epithelial cells differentiated in a cell sheet constructed by magnetic nanotechnology" by Koto et al. is licensed and used under CC BY. Excerpt from original

fabricated via Mag-TE, epithelial-mesenchymal interactions were induced between DEC and DMC layers in the CC sheet, and DECs differentiated into enamel-secreting ameloblasts in the sheet.

3.2 Spheroid modulation with magnetic based 3D cell culture platform

Microfluidics [114–116], polymer matrices [117, 118], HD [119–122], and centrifugation [123–125] are utilized to make spheroids. However, these methods have several limitations, including difficulties in changing the culture media, limited cell suspension volume, expensive special plates for spheroid formation, and difficulties in scaling up these methods [4]. Additionally, an external force used as a mechanical stimulus could affect the behavior of cells during and after spheroid formation. In some methods, such as HD, an active force for cell contact and aggregation is not enough [121] and could limit the spatial control of the cells and delay the spheroid formation process. As mentioned earlier, magnetic fields show the potential for the indirect application of forces onto magnetically labeled cells with spatial and temporal control [126]. Jafari et al. reported that different shapes and sizes of 3D cellular aggregate formation were induced by utilizing various magnetic field configurations [126]. The authors used magnetic particle (MP)-labeled NIH 3T3 fibroblasts and 3T3-L1 preadipocytes. Cylindrical permanent magnets were used under the culture plates (Fig. 6A) to produce uniform and stable cell spheroids, providing a sufficient active force for enhancing cell–cell interactions and reducing the formation time of cell spheroids (Fig. 6B). This method produced highly dense and more symmetric spheroid structures compared to the commonly used

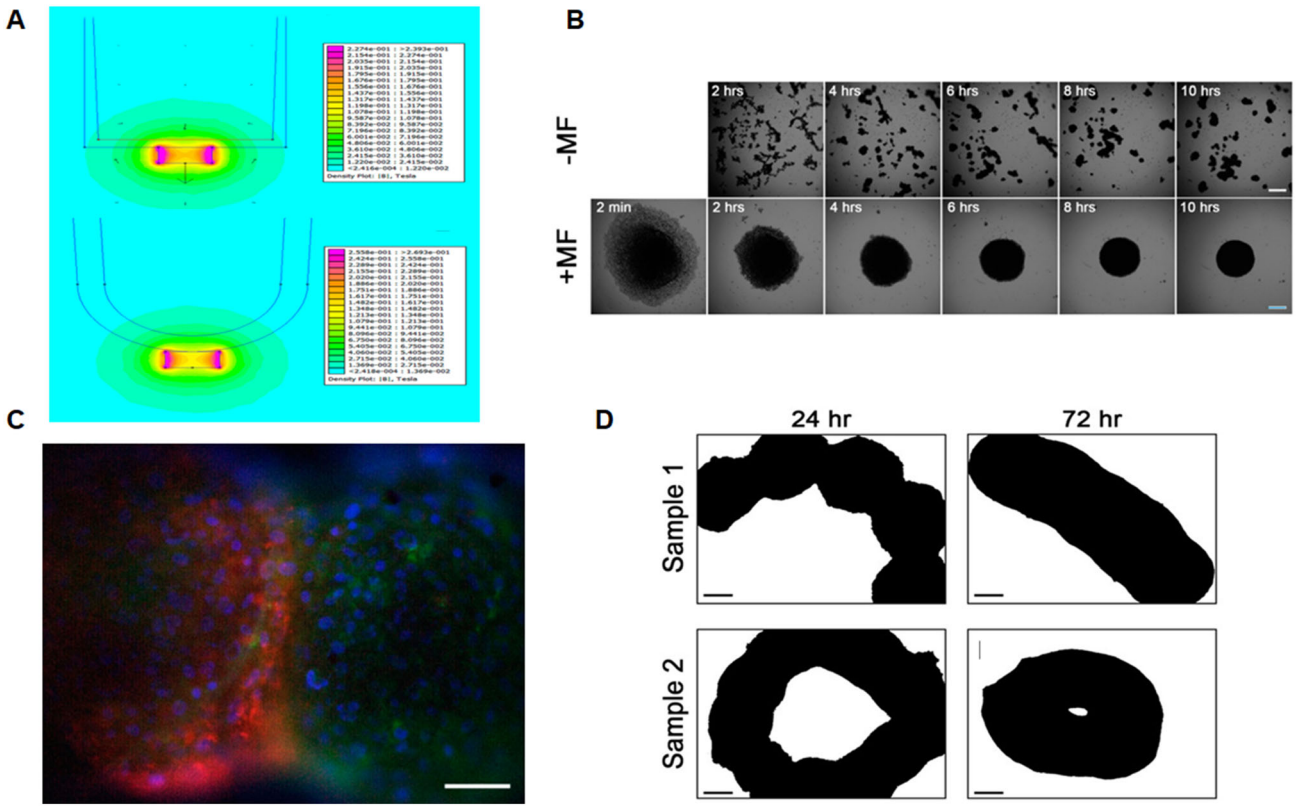

Fig. 6 Remote control of the formation of uniform 3D cell constructs using magnetic forces. **A** FEMM simulation results showing the magnetic field generated by M21 (D = 2 mm, h = 1 mm) magnets under flat- (top) and round-bottom (bottom) plates. The color map varies from 0.2 × 10–5 to 0.2 T. **B** Formation of 3T3-L1 cell spheroids in the presence (+ MF) and absence (− MF) of a magnetic field applied after different times in culture (scale bars: 300 μm). **C** Fluorescence image from two merged spheroids after 24 h of culture. 3T3-L1 spheroids were first stained with red and green CellTrackers, separately and then cultured together for 24 h in the presence of MF. The nuclei were stained with DAPI (blue) and visualized by fluorescence microscopy (scale bar: 100 μm). **D** Inverted microscopy images after fusion of 5 (sample 1) and 10 (sample 2) 3T3-L1 cell spheroids on ring magnets (R211) for 24 h (scale bar: 200 μm). "Remote control in formation of 3D multicellular assemblies using magnetic forces" by Jafari et al. is licensed and used under CC BY. Excerpt from original

centrifugation method. Magnetic force and centrifugation were applied to the cells, enhancing the formation of spheroids. The fusion of spheroids occurred due to magnetic forces. Two or four spheroids were seeded into a single well, with a magnet located under the plate. Spheroid fusion then occurred, and some cells migrated from one spheroid to another after 24 h (Fig. 6C). Experiments were also conducted to form spheroids of different shapes based on the presence of magnetic forces. A ring-type magnet was placed for 24 h and then removed. The constructs retained their shape when they were exposed to magnetic fields for up to 24 h. When the magnet was removed, aggregates began to remodel and change shape into rod-like or doughnut shapes, which was dependent on the number of spheroids initially used. In summary, magnetic fields could manipulate spheroid formation and structure (Fig. 6D) [126].

3.3 Self assembled 3D cell cultures with magnetic based 3D cell culture platform by magnetic levitation

In general, MSCs are isolated from bone marrow (BM) and cultured as 2D monolayers [127]. However, the 2D-culturing of MSCs induces the loss of differentiation potential and senescence after several generations [128, 129]. And quiescence and multipotency, which are stem cell properties, were lost during culturing [130]. The microenvironment in which MSCs reside is important for maintaining MSC function and preventing differentiation [131]. MSCs niche which termed MSCs reside in a protective site in the BM, and the BM environment is essential for maintaining the MSC phenotype [127]. Lewis et al. fabricated MSC multicellular spheroids with magnetic nanoparticles and implanted them into collagen gel, which had a stiffness similar to the *in vivo* BM microenvironment, to maintain MSC properties by magnetic levitation [127]. Collagen

type I is located on the endosteal surface and endosteal marrow, which is a stem cell niche site and abundant in BM [132]. MSCs were seeded in 24-well culture plates to make MSC spheroids. After 24 h of culture, the MSCs were treated with green fluorescently labeled magnetic iron oxide (FeO_3) at 0.1 mg/mL and incubated for 30 min directly above a magnetic plate to enhance cell internalization. The cells were detached from the plates with trypsin and transferred to a 6-well plate, with a single neodymium magnet located above each well for inducing cell aggregation. In this condition, spheroids formed within 24 h. Transmission electron microscopy showed nanoparticles successfully internalized into MSCs, and scanning electron microscopy confirmed MSC spheroid formation with spherical structures (Fig. 7A). After spheroid formation in 24 h of culture, the spheroids were transferred to a 24-well plate, and a collagen gel solution was added. The culture plate was incubated at 37 °C for gelation. A magnet was placed over each well for the first 24 h. After 7 days of culture, stem cell marker expression was analyzed by immunohistochemistry (Fig. 7B). MSCs cultured in a monolayer were used as controls. MSCs in the spheroid form maintained STRO-1 expression and increased nestin and SDF1-α expression compared to monolayer-cultured MSCs (Fig. 7B). STRO-1 is a marker used to isolate MSC colony-forming units [133]. STRO-1 expression in the spheroids suggested that the spheroid system prevented differentiation and sustained the stem cell population as it would be in the BM. Nestin is a cytoskeletal component that hematopoietic stem cells (HSC)-supportive subset of MSCs in the BM [134]. SDF1-α is homing factor correlated with HSC mobilization and homing to the BM niche [135]. Enhanced nestin and SDF1-α expression suggested that this spheroid culture system was similar to the *in vivo*

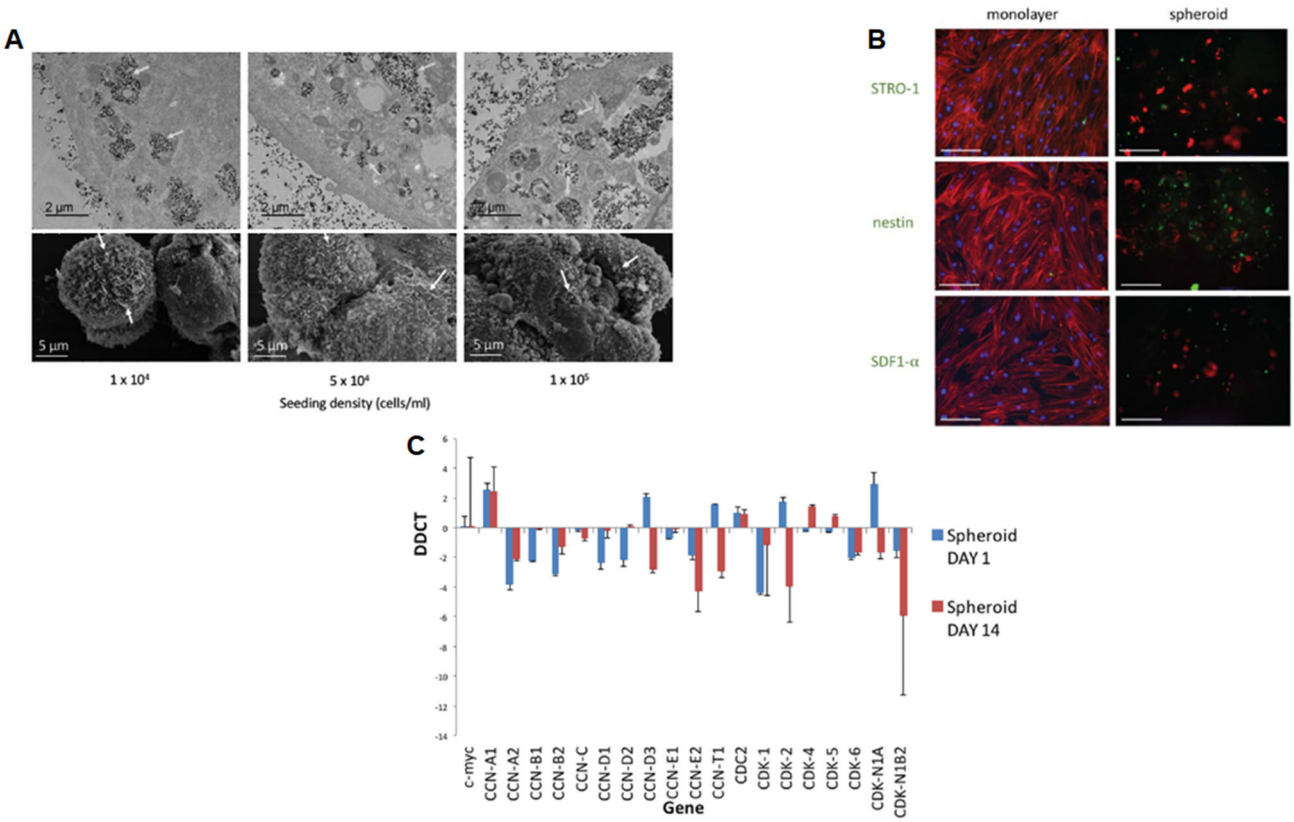

Fig. 7 Multicellular MSC spheroids in a magnetic-based 3D culture system cultured in collagen gel to maintain phenotype and quiescence. **A** Transmission electron micrographs clearly indicate nanoparticles located in vesicles within the cell cytoplasm (top), while scanning electron micrographs show the general morphology and dimensions of the multicellular MSC spheroids (bottom). The top arrows indicate nanoparticles within vesicles. The bottom arrows indicate cellular projections. **B** Immunohistochemistry was performed on MSCs grown in either monolayers or spheroid culture systems for 7 days. DAPI (blue) = DNA/nuclei, TRITC (red) = phalloidin (actin); fluorescein isothiocyanate (FITC) (green) = STRO-1, nestin or SDF1-α, respectively. Scale bars = 200 µm. **C** Analysis of cell cycle gene expression in spheroids. Cell cycle gene analysis of spheroids on day 1 and day 14 normalized to the corresponding monolayers. The graph shows the expression of cyclins and cyclin-dependent kinases involved in the cell cycle process. The graph shows the fold-change in gene expression identified by delta-delta-Ct (DDCT) analysis in spheroids compared to monolayer culture. CCN = cyclin and CDK = cyclin-dependent kinase; n = 3, technical replicates. "Magnetically levitated mesenchymal stem cell spheroids cultured with a collagen gel maintain phenotype and quiescence" by Lewis et al. is licensed and used under CC BY. Excerpt from original

niche. Finally, the cell cycle of MSCs cultured in spheroid was analyzed by gene expression (Fig. 7C) on days 1 and 14. The genes shown in the graph were associated with the cell cycle. The fold-change in gene expression in MSC spheroids was normalized to the expression in monolayer-cultured MSCs. Interestingly, gene expression in the MSC spheroids was downregulated on day 1 and decreased on day 14, indicating that the cell cycling of MSCs in spheroid forms progressed slowly (Fig. 7C). Decreased cyclin C in spheroids indicated that more cells remained in the G0 phase. D1 and D2 cyclin expression was lower in the spheroids on day 1 and recovered on day 14, cyclin D expression was increased on day 1 and decreased on day 14, CDK4 expression was decreased on day 1 and increased on day 14, and CDK6 expression was decreased on days 1 and 14. This indicated that insufficient cyclin D accumulation induced the cells to leave the G1 phase and enter the S phase. Cyclin E2 expression was downregulated in the spheroids on days 1 and 14, and CDK2 expression was increased on day 1 and decreased on day 14, indicating that a small number of cells had entered the S phase. In conclusion, MSC spheroids were successfully fabricated with magnetic forces, and this spheroid culture system with type I collagen gel was a potential *in vitro* BM stem cell niche platform.

Magnetic levitation can be induced by positive or negative magnetophoresis [136]. However, positive meganetophoersis, such as the magnetic bead-labeling technique, can only affect the surface of a subject without inducing weightlessness [75, 137]. In contrast, negative meganetophoersis can mimic weightlessness [107]. With negative magnetophoresis, the gravitational force on the subject can be compensated by the counteracting force and induce weightlessness. Anil-Inevi et al. [136] used this magnetic levitation technique with negative magnetophoresis for long-term levitated cell culture and fabricated a 3D in situ cellular assembly model. A gadolinium (Gd^{3+})-based solution was used to induce cell levitation because it was inexpensive. In addition, it could induce the assembly of *ex-situ* spheroids [138, 139]. The magnetic levitation platform in this experiment consisted of two high-grade (N52) neodymium magnets [136]. The two magnets were located at a distance of 1.5 mm from the same pole, facing each other, and there was a microcapillary channel between the two magnets. There were also mirrors at 45° for real-time inverted microscopy imaging. The magnetic levitation device consisted of a photoreactive resin printed using a 3D printer (Fig. 8A). As the magnetic susceptibility of the cells and surrounding paramagnetic medium was different, cells suspended in the paramagnetic medium moved away from a high magnetic field, such as a magnet close to the magnets in a low magnetic field. Until the cells reached an equilibrium position, buoyancy (F_b), fluidic drag (F_d), inertial (F_i), and magnetic forces (F_{mag}) affected the cells (Fig. 8A). When the cells were close to the equilibrium position, the velocity of the cells, and thus F_i and F_d, decreased. Therefore, the cells levitated at the position that F_b and F_{mag} equilibrate in opposite directions. The concentration and composition of the Gd^{3+}-based solution were optimized for weightlessness culturing to test self-assembled 3D cell cultures with magnetic levitation. Various types (Gd-DOTA, Gd-DTPA, Gd-DTPA-BMA, Gd-BT-DO3A, and Gd-BOPTA) and concentrations (0, 10, 25, 50, 100, and 200 mM) of Gd-based solutions were used to treat D1 ORL UVA, a BMSC stem cell line and MDA-MB-231 cells, and the location of the cells from the bottom of the capillary after 10 min of levitation was analyzed to find the lower concentration of Gd^{3+} that induced cell levitation and reached steady-state (Fig. 8B). Cell levitation height was increased with increasing concentrations (Fig. 8B). Through cell viability determinations 72 h after Gd-based solution treatment and levitation assays, 100 mM Gd-BT-DO3A treatment was chosen for the levitation experiments because it offered greater levitation height and cell viability. Then, the effect of cell number on the morphology of cell clusters formed under microgravity conditions was investigated. After 5000, 50,000, and 500,000 cells were levitated for 48 h, their morphology was analyzed. After 24 h, the area, perimeter, elongation, thickness, and length of the cellular constructure were not significantly different. However, after 48 h, when cell numbers had increased, these parameters also increased. Finally, the self-assembly of different cell types with magnetic levitation was evaluated with D1 ORL UVA^{eGFP} (green) cells and MDA-MB-231^{dsRed} (red) cells. Before biphasic cluster formation, D1 ORL UVA^{eGFP} cells and MDA-MB-231^{dsRed} cells were utilized separately for levitated 3D clusters and analyzed. D1 ORL UVA^{eGFP} and MDA-MB-231^{dsRed} 3D clusters showed similar levitation heights. However, MDA-MB-231 clusters had larger area, perimeter, elongation, and length than D1 ORL UVA cells. For biphasic assembly, D1 ORL UVA^{eGFP} cells and MDA-MB-231^{dsRed} cells were loaded with different L1, L2, and L3 strategies. With L1, D1 ORL UVA^{eGFP} cells and MDA-MB-231^{dsRed} cells were simultaneously loaded. With L2, MDA-MB-231^{dsRed} cells were loaded onto D1 ORL UVA^{eGFP} cells. With L3, D1 ORL UVA^{eGFP} cells were loaded onto MDA-MB-231^{dsRed} cells. With the L1 strategy, cells showed completely random positions in the cluster (Fig. 8D). With the L2 strategy, MDA-MB-231^{dsRed} cells were loosely distributed on the surface of D1 ORL UVA^{eGFP} cells (Fig. 8D). Interestingly, with the L3 strategy, patterned clusters formed, with D1 ORL UVA^{eGFP} cells aggregated and located in gaps within MDA-MB-231^{dsRed} clusters. In summary, the magnetic levitation system with Gd was a fast and convenient method to simulate microgravity conditions. This

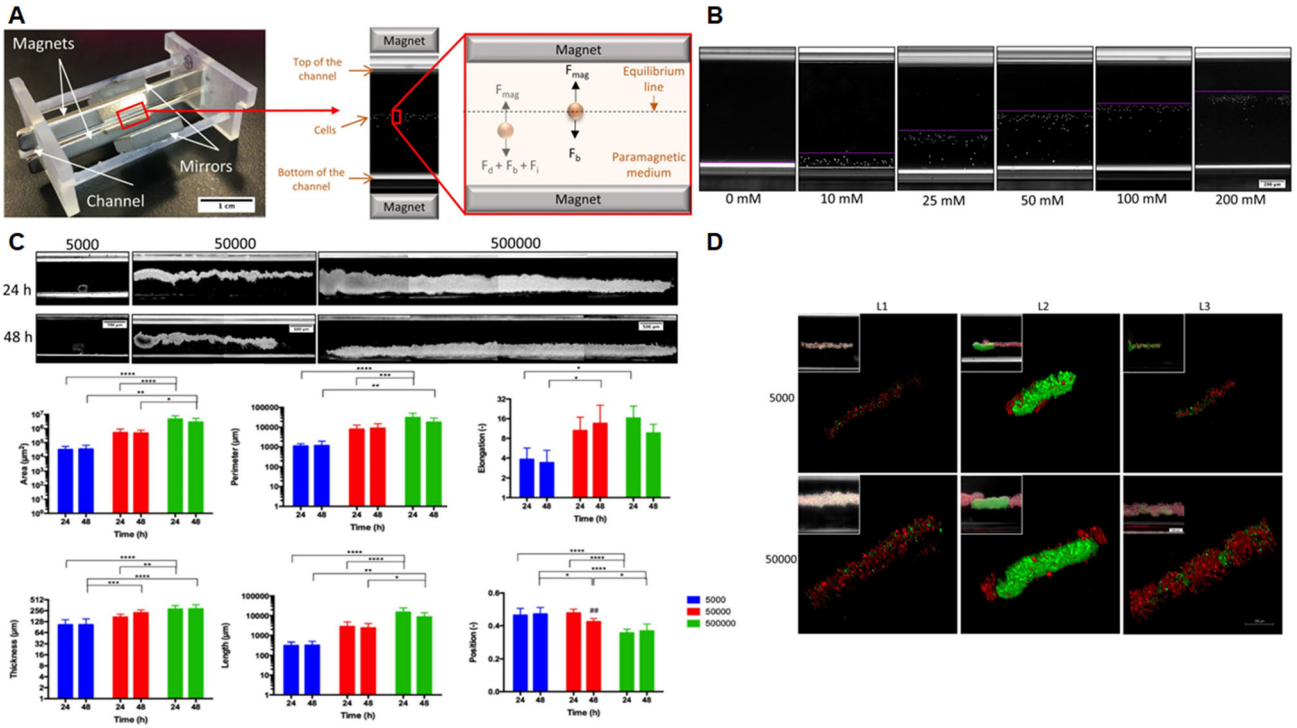

Fig. 8 **A** Photograph of the magnetic levitation platform and schematic of the device, illustrating forces acting on cells until equilibrium: fluidic drag force (F_d), inertial force (F_i), buoyancy force (F_b), and magnetic force, F_{mag}, and at the equilibrium position, F_{mag} and F_b. **A** A microcapillary channel, in which cells are levitated and cultured, was placed between two permanent neodymium magnets whose same negative poles were facing each other. Mirrors were placed at each open side of the channel at 45° and used to visualize cells in the channel using conventional microscopy systems. **B** Micrographs of levitated cells after 10 min of levitation in medium containing Gd-BT-DO3A at varying concentrations (0, 10, 25, 50, 100, and 200 mM). The lines show the upper level of the levitated cell population. Scale bar: 200 µm. **C** 3D cellular organization of D1 ORL UVA cells under microgravity. **C** Cellular assembly of D1 ORL UVA^{eGFP} and MDA-MB-231^{dsRed} cells under microgravity. Scale bar: 200 µm. "Biofabrication of in situ self-assembled 3D cell cultures in a weightlessness environment generated using magnetic levitation" by Anil-Inevi et al. is licensed and used under CC BY. Excerpt from original

multitype cellular cluster assembly method could also be utilized in biomedical studies.

4 Challenges and future perspective

As reviewed in this article, acoustic and magnetic technologies can be integrated with 3D cell culture systems and used efficiently to build 3D models, such as cell spheroids. However, some challenges must be considered before they can be used as more advanced technologies in life science fields.

One of the factors that should be considered when using the acoustic-based 3D cell culture platform for cell culture is temperature control [140]. SAWs can increase the temperature of the culture environment within devices [141–145] due to mechanical damping and the Joule effect [146]. Therefore, it is important to set SAW parameters within appropriate ranges so that the resulting temperature increase in the culture environment does not affect cell viability. Several studies reported the optimal parameters of acoustic systems for reducing cell damage [147, 148]. However, it is difficult to apply the optimal parameters of one system to other systems since the parameters were optimized for specific systems. Thus, investigating more standardized parameters would help to broaden the use of acoustic systems in biological fields [35].

The biocompatibility of materials used in magnetic technologies should also be considered when the technologies are applied to cell culture. In the case of positive magnetophoresis, labeling cells with MNPs can cause cytotoxicity [76] or unintended cellular responses [149], as described above. To avoid the bio-incompatibility issues of MNPs, negative magnetophoresis using paramagnetic salt can be chosen. However, a highly concentrated paramagnetic salt solution, which is required for effective magnetophoresis due to the low magnetic susceptibility of paramagnetic salt, can induce cell dehydration through osmotic pressure [150, 151]. Therefore, further studies on the biocompatibility of MNPs and optimization of paramagnetic salt solutions should be performed.

Acoustic and magnetic technologies are widely used in the fields of biology and medicine. In terms of tissue engineering, acoustic technologies have shown the potential to overcome the limitations of 3D bio-printing. 3D bio-printing cannot fabricate tissues with high cell densities and physiologically required structural complexity. In contrast, acoustics act on hydrogel-located cells and arrange the cells into desired structures, creating biomimetic tissue structures with high cell densities [152]. Acoustic holography [153, 154] and acoustic vortex [155] techniques could be introduced to pattern more complex structures. Also, various 3D bio-printing and acoustic technologies have been integrated with each other to further improve the mimicking of living tissue [152]. This will lead to the development of tissue engineering, as well. Similarly, magnetic technology has also been incorporated and utilized in 4D bio-printing. Tissue constructs consisting of alternate stacking on unidirectionally aligned collagen fibers by magnetic properties and randomly arranged collagen fibers exhibited improved cartilage potential [156]. Magnetic fields have also been used to modulate cellular behaviors, such as mitochondrial dynamics, gene expression, and cytoskeletal assembly, by manipulating intracellular superparamagnetic nanoparticles [157–159]. In this context, we could expect the development of remote magneto-genetic switches for tissue engineering from further studies of magneto-genetics [160].

5 Conclusion

The 2D culture method shows major limitations, including dissimilarity with natural tissue forms without mimicking the *in vivo* microenvironment. Therefore, 3D cell culture is important for tissue engineering. Scaffold-free 3D cell culture methods, including hanging drops and forced floating methods, show the drawbacks of being labor-intensive and time-consuming. Therefore, external physical stimulation, such as acoustic and magnetic force-based 3D cell culture platforms, have been developed. Acoustic, magnetic force-based 3D cell culture platforms require less labor. Various 3D cell types, such as spheroids, cell fibers, and vascular networks, can be successfully formed by acoustic wave or magnetic field-based 3D cell culture platforms. These cells showed enhanced behaviors and formed 3D cell aggregates in a short time. Based on improved cell aggregate biological abilities, a physical stimuli-based 3D cell culture platform could be a promising tool for tissue engineering.

Acknowledgements This study was supported by 2022 Research Grant from Kangwon National University (202202400001) (T.-J. L.) and National Research Foundation of Korea (NRF) grant funded by the Korea government(MSIT) (No. NRF-2022R1C1C2011617) (H.-K. J.)

Declarations

Conflicts of interest The authors have no conflicts of interest relevant to this study to disclose.

Ethical statement No animal experiments were carried out for this article.

References

1. Costa EC, Moreira AF, de Melo-Diogo D, Gaspar VM, Carvalho MP, Correia IJ. 3D tumor spheroids: an overview on the tools and techniques used for their analysis. Biotechnol Adv. 2016;34:1427–41.
2. Langhans SA. Three-dimensional in vitro cell culture models in drug discovery and drug repositioning. Front Pharmacol. 2018;9:6.
3. Antoni D, Burckel H, Josset E, Noel G. Three-dimensional cell culture: a breakthrough in vivo. Int J Mol Sci. 2015;16:5517–27.
4. Breslin S, O'Driscoll L. Three-dimensional cell culture: the missing link in drug discovery. Drug Discov Today. 2013;18:240–9.
5. Kapałczyńska M, Kolenda T, Przybyła W, Zajączkowska M, Teresiak A, Filas V, et al. 2D and 3D cell cultures - a comparison of different types of cancer cell cultures. Arch Med Sci. 2018;14:910–9.
6. von der Mark K, Gauss V, von der Mark H, Müller P. Relationship between cell shape and type of collagen synthesised as chondrocytes lose their cartilage phenotype in culture. Nature. 1977;267:531–2.
7. Petersen OW, Rønnov-Jessen L, Howlett AR, Bissell MJ. Interaction with basement membrane serves to rapidly distinguish growth and differentiation pattern of normal and malignant human breast epithelial cells. Proc Natl Acad Sci U S A. 1992;89:9064–8.
8. Mahmud G, Campbell C, Bishop KJM, Komarova YA, Chaga O, Soh S, et al. Directing cell motions on micropatterned ratchets. Nature Phys. 2009;5:606–12.
9. Kilian KA, Bugarija B, Lahn BT, Mrksich M. Geometric cues for directing the differentiation of mesenchymal stem cells. Proc Natl Acad Sci U S A. 2010;107:4872–7.
10. Debnath J, Brugge JS. Modelling glandular epithelial cancers in three-dimensional cultures. Nat Rev Cancer. 2005;5:675–88.
11. Nelson CM, Bissell MJ. Of extracellular matrix, scaffolds, and signaling: tissue architecture regulates development, homeostasis, and cancer. Annu Rev Cell Dev Biol. 2006;22:287–309.
12. Mseka T, Bamburg JR, Cramer LP. ADF/cofilin family proteins control formation of oriented actin-filament bundles in the cell body to trigger fibroblast polarization. J Cell Sci. 2007;120:4332–44.
13. Weaver VM, Lelièvre S, Lakins JN, Chrenek MA, Jones JC, Giancotti F, Werb Z, Bissell MJ. beta4 integrin-dependent formation of polarized three-dimensional architecture confers resistance to apoptosis in normal and malignant mammary epithelium. Cancer Cell. 2002;2:205–16.
14. Meyers J, Craig J, Odde DJ. Potential for control of signaling pathways via cell size and shape. Curr Biol. 2006;16:1685–93.
15. Joyce JA, Pollard JW. Microenvironmental regulation of metastasis. Nat Rev Cancer. 2009;9:239–52.

16. Trédan O, Galmarini CM, Patel K, Tannock IF. Drug resistance and the solid tumor microenvironment. J Natl Cancer Inst. 2007;99:1441–54.
17. Hutchinson L, Kirk R. High drug attrition rates–where are we going wrong? Nat Rev Clin Oncol. 2011;8:189–90.
18. Lovitt CJ, Shelper TB, Avery VM. Advanced cell culture techniques for cancer drug discovery. Biology. 2014;3:345–67.
19. Knight E, Przyborski S. Advances in 3D cell culture technologies enabling tissue-like structures to be created in vitro. J Anat. 2015;227:746–56.
20. Cukierman E, Pankov R, Yamada KM. Cell interactions with three-dimensional matrices. Curr Opin Cell Biol. 2002;14:633–9.
21. Bokhari M, Carnachan RJ, Cameron NR, Przyborski SA. Culture of HepG2 liver cells on three dimensional polystyrene scaffolds enhances cell structure and function during toxicological challenge. J Anat. 2007;211:567–76.
22. Sun T, Jackson S, Haycock JW, MacNeil S. Culture of skin cells in 3D rather than 2D improves their ability to survive exposure to cytotoxic agents. J Biotechnol. 2006;122:372–81.
23. Ridky TW, Chow JM, Wong DJ, Khavari PA. Invasive three-dimensional organotypic neoplasia from multiple normal human epithelia. Nat Med. 2010;16:1450–5.
24. Boghaert ER, Lu X, Hessler PE, McGonigal TP, Oleksijew A, Mitten MJ, et al. The volume of three-dimensional cultures of cancer cells invitro influences transcriptional profile differences and similarities with monolayer cultures and xenografted tumors. Neoplasia. 2017;19:695–706.
25. Cacciamali A, Villa R, Dotti S. 3D cell cultures: evolution of an ancient tool for new applications. Front Physiol. 2022;13:836480.
26. Jensen C, Teng Y. Is it time to start transitioning from 2D to 3D cell culture? Front Mol Biosci. 2020;7:33.
27. Barbosa MAG, Xavier CPR, Pereira RF, Petrikaitė V, Vasconcelos MH. 3D cell culture models as recapitulators of the tumor microenvironment for the screening of anti-cancer drugs. Cancers. 2021;14:190.
28. Chen MY, Skewes J, Desselle M, Wong C, Woodruff MA, Dasgupta P, et al. Current applications of three-dimensional printing in urology. BJU Int. 2020;125:17–27.
29. Shokoohmand A, Ren J, Baldwin J, Atack A, Shafiee A, Theodoropoulos C, et al. Microenvironment engineering of osteoblastic bone metastases reveals osteomimicry of patient-derived prostate cancer xenografts. Biomaterials. 2019;220:119402.
30. Pinto B, Henriques AC, Silva PMA, Bousbaa H. Three-dimensional spheroids as in vitro preclinical models for cancer research. Pharmaceutics. 2020;12:1186.
31. Agrawal G, Ramesh A, Aishwarya P, Sally J, Ravi M. Devices and techniques used to obtain and analyze three-dimensional cell cultures. Biotechnol Prog. 2021;37:e3126.
32. Meng L, Cai F, Li F, Zhou W, Niu L, Zhen H. Acoustic tweezers. J Phys D Appl Phys. 2019;52:273001.
33. Destgeer G, Sung HJ. Recent advances in microfluidic actuation and micro-object manipulation via surface acoustic waves. Lab Chip. 2015;15:2722–38.
34. Baresch D, Thomas JL, Marchiano R. Observation of a single-beam gradient force acoustical trap for elastic particles: acoustical tweezers. Phys Rev Lett. 2016;116:024301.
35. Ozcelik A, Rufo J, Guo F, Gu Y, Li P, Lata J, et al. Acoustic tweezers for the life sciences. Nat Methods. 2018;15:1021–8.
36. Olofsson K, Hammarström B, Wiklund M. Ultrasonic based tissue modelling and engineering. Micromachines (Basel). 2018;9:594.
37. Friend J, Yeo LY. Microscale acoustofluidics: microfluidics driven via acoustics and ultrasonics. Rev Mod Phys. 2011;83:647–704.
38. Länge K, Rapp BE, Rapp M. Surface acoustic wave biosensors: a review. Anal Bioanal Chem. 2008;391:1509–19.
39. Lenshof A, Evander M, Laurell T, Nilsson J. Acoustofluidics 5: Building microfluidic acoustic resonators. Lab Chip. 2012;12:684–95.
40. Luong TD, Nguyen NT. Surface acoustic wave driven microfuidics: a review. Micro Nanosyst. 2010;2:217–25.
41. Ding X, Li P, Lin SC, Stratton ZS, Nama N, Guo F, et al. Surface acoustic wave microfluidics. Lab Chip. 2013;13:3626–49.
42. Wu Y, Ao Z, Chen B, Muhsen M, Bondesson M, Lu X, et al. Acoustic assembly of cell spheroids in disposable capillaries. Nanotechnology. 2018;29:504006.
43. Dumy G, Jeger-Madiot N, Benoit-Gonin X, Mallouk TE, Hoyos M, Aider JL. Acoustic manipulation of dense nanorods in microgravity. Microgravity Sci Technol. 2020;32:1159–74.
44. Castro LA, Hoyos M. Determination of the secondary bjerknes force in acoustic resonators on ground and in microgravity conditions. Microgravity Sci Technol. 2016;28:11–8.
45. Silva GT, Lopes JH, Leão-Neto JP, Nichols MK, Drinkwater BW. Particle patterning by ultrasonic standing waves in a rectangular cavity. Phys Rev Applied. 2019;11:054044.
46. Laurell T, Petersson F, Nilsson A. Chip integrated strategies for acoustic separation and manipulation of cells and particles. Chem Soc Rev. 2007;36:492–506.
47. Jeger-Madiot N, Arakelian L, Setterblad N, Bruneval P, Hoyos M, Larghero J, et al. Self-organization and culture of mesenchymal stem cell spheroids in acoustic levitation. Sci Rep. 2021;11:8355.
48. Fang XZ, Zhou T, Xu JQ, Wang YX, Sun MM, He YJ, et al. Structure, kinetic properties and biological function of mechanosensitive Piezo channels. Cell Biosci. 2021;11:13.
49. Passini FS, Jaeger PK, Saab AS, Hanlon S, Chittim NA, Arlt MJ, et al. Shear-stress sensing by PIEZO1 regulates tendon stiffness in rodents and influences jumping performance in humans. Nat Biomed Eng. 2021;5:1457–71.
50. Pardo-Pastor C, Rubio-Moscardo F, Vogel-González M, Serra SA, Afthinos A, Mrkonjic S, et al. Piezo2 channel regulates RhoA and actin cytoskeleton to promote cell mechanobiological responses. Proc Natl Acad Sci U S A. 2018;115:1925–30.
51. Pathak MM, Nourse JL, Tran T, Hwe J, Arulmoli J, Le DT, et al. Stretch-activated ion channel Piezo1 directs lineage choice in human neural stem cells. Proc Natl Acad Sci U S A. 2014;111:16148–53.
52. Wei L, Mousawi F, Li D, Roger S, Li J, Yang X, et al. Adenosine triphosphate release and P2 receptor signaling in piezo1 channel-dependent mechanoregulation. Front Pharmacol. 2019;10:1304.
53. Im GB, Kim YJ, Lee TI, Bhang SH. Subaqueous free-standing 3D cell culture system for ultrafast cell compaction, mechano-inductive immune control, and improving therapeutic angiogenesis. Bioeng Transl Med. 2022;e10438.
54. Mende N, Kuchen EE, Lesche M, Grinenko T, Kokkaliaris KD, Hanenberg H, et al. CCND1-CDK4-mediated cell cycle progression provides a competitive advantage for human hematopoietic stem cells in vivo. J Exp Med. 2015;212:1171–83.
55. Strzalka W, Ziemienowicz A. Proliferating cell nuclear antigen (PCNA): a key factor in DNA replication and cell cycle regulation. Ann Bot. 2011;107:1127–40.
56. Karar J, Maity A. PI3K/AKT/mTOR pathway in angiogenesis. Front Mol Neurosci. 2011;4:51.

57. Chen S, Shi J, Zhang M, Chen Y, Wang X, Zhang L, et al. Mesenchymal stem cell-laden anti-inflammatory hydrogel enhances diabetic wound healing. Sci Rep. 2015;5:18104.
58. Krzyszczyk P, Schloss R, Palmer A, Berthiaume F. The role of macrophages in acute and chronic wound healing and interventions to promote pro-wound healing phenotypes. Front Physiol. 2018;9:419.
59. Gherardini L, Cousins CM, Hawkes JJ, Spengler J, Radel S, Lawler H, et al. A new immobilisation method to arrange particles in a gel matrix by ultrasound standing waves. Ultrasound Med Biol. 2005;31:261–72.
60. Koo KI, Lenshof A, Huong LT, Laurell T. Acoustic cell patterning in hydrogel for three-dimensional cell network formation. Micromachines (Basel). 2020;12:3.
61. Comeau ES, Hocking DC, Dalecki D. Ultrasound patterning technologies for studying vascular morphogenesis in 3D. J Cell Sci. 2017;130:232–42.
62. Hitchcock T, Niklason L. Lymphatic tissue engineering: progress and prospects. Ann N Y Acad Sci. 2008;1131:44–9.
63. Radisic M, Yang L, Boublik J, Cohen RJ, Langer R, Freed LE, Vunjak-Novakovic G. Medium perfusion enables engineering of compact and contractile cardiac tissue. Am J Physiol Heart Circ Physiol. 2004;286:H507–16.
64. Asakawa N, Shimizu T, Tsuda Y, Sekiya S, Sasagawa T, Yamato M, Fukai F, Okano T. Pre-vascularization of in vitro three-dimensional tissues created by cell sheet engineering. Biomaterials. 2010;31:3903–9.
65. Laschke MW, Vollmar B, Menger MD. Inosculation: connecting the life-sustaining pipelines. Tissue Eng Part B Rev. 2009;15:455–65.
66. Armstrong JPK, Puetzer JL, Serio A, Guex AG, Kapnisi M, Breant A, et al. Engineering anisotropic muscle tissue using acoustic cell patterning. Adv Mater. 2018;30:e1802649.
67. Garvin KA, Dalecki D, Hocking DC. Vascularization of three-dimensional collagen hydrogels using ultrasound standing wave fields. Ultrasound Med Biol. 2011;37:1853–64.
68. Garvin KA, Hocking DC, Dalecki D. Controlling the spatial organization of cells and extracellular matrix proteins in engineered tissues using ultrasound standing wave fields. Ultrasound Med Biol. 2010;36:1919–32.
69. Garvin KA, Dalecki D, Yousefhussien M, Helguera M, Hocking DC. Spatial patterning of endothelial cells and vascular network formation using ultrasound standing wave fields. J Acoust Soc Am. 2013;134:1483–90.
70. Hu X, Zheng J, Hu Q, Liang L, Yang D, Cheng Y, et al. Smart acoustic 3D cell construct assembly with high-resolution. Biofabrication. 2022;14:045003.
71. Sensenig R, Sapir Y, MacDonald C, Cohen S, Polyak B. Magnetic nanoparticle-based approaches to locally target therapy and enhance tissue regeneration in vivo. Nanomedicine (Lond). 2012;7:1425–42.
72. Wang A, Madden LA, Paunov VN. Advanced biomedical applications based on emerging 3D cell culturing platforms. J Mater Chem B. 2020;8:10487–501.
73. Yaman S, Anil-Inevi M, Ozcivici E, Tekin HC. Magnetic force-based microfluidic techniques for cellular and tissue bioengineering. Front Bioeng Biotechnol. 2018;6:192.
74. Frasca G, Gazeau F, Wilhelm C. Formation of a three-dimensional multicellular assembly using magnetic patterning. Langmuir. 2009;25:2348–54.
75. Souza GR, Molina JR, Raphael RM, Ozawa MG, Stark DJ, Levin CS, et al. Three-dimensional tissue culture based on magnetic cell levitation. Nat Nanotechnol. 2010;5:291–6.
76. Tomitaka A, Koshi T, Hatsugai S, Yamada T, Takemura Y. Magnetic characterization of surface-coated magnetic nanoparticles for biomedical application. J Magn Magn Mater. 2011;323:1398–403.
77. Mattix B, Olsen TR, Gu Y, Casco M, Herbst A, Simionescu DT, et al. Biological magnetic cellular spheroids as building blocks for tissue engineering. Acta Biomater. 2014;10:623–9.
78. Xue L, Deng D, Sun J. Magnetoferritin: process, prospects, and their biomedical applications. Int J Mol Sci. 2019;20:2426.
79. Correia Carreira S, Armstrong JP, Seddon AM, Perriman AW, Hartley-Davies R, Schwarzacher W. Ultra-fast stem cell labelling using cationised magnetoferritin. Nanoscale. 2016;8:7474–83.
80. Charlton JR, Pearl VM, Denotti AR, Lee JB, Swaminathan S, Scindia YM, et al. Biocompatibility of ferritin-based nanoparticles as targeted MRI contrast agents. Nanomedicine. 2016;12:1735–45.
81. Dzamukova M, Naumenko E, Rozhina EV, Trifonov AA, Fakhrullin RF. Cell surface engineering with polyelectrolyte-stabilized magnetic nanoparticles: a facile approach for fabrication of artificial multicellular tissue-mimicking clusters. Nano Res. 2015;8:2515–32.
82. Sarigil O, Anil-Inevi M, Firatligil-Yildirir B, Unal YC, Yalcin-Ozuysal O, Mese G, et al. Scaffold-free biofabrication of adipocyte structures with magnetic levitation. Biotechnol Bioeng. 2021;118:1127–40.
83. Parfenov VA, Koudan EV, Bulanova EA, Karalkin PA, Das Pereira F, Norkin NE, et al. Scaffold-free, label-free and nozzle-free biofabrication technology using magnetic levitational assembly. Biofabrication. 2018;10:034104.
84. Ito A, Takizawa Y, Honda H, Hata K, Kagami H, Ueda M, et al. Tissue engineering using magnetite nanoparticles and magnetic force: heterotypic layers of cocultured hepatocytes and endothelial cells. Tissue Eng. 2004;10:833–40.
85. Ishii M, Shibata R, Shimizu Y, Yamamoto T, Kondo K, Inoue Y, et al. Multilayered adipose-derived regenerative cell sheets created by a novel magnetite tissue engineering method for myocardial infarction. Int J Cardiol. 2014;175:545–53.
86. Peyman SA, Kwan EY, Margarson O, Iles A, Pamme N. Diamagnetic repulsion–a versatile tool for label-free particle handling in microfluidic devices. J Chromatogr A. 2009;1216:9055–62.
87. Zhu T, Marrero F, Mao L. Continuous separation of non-magnetic particles inside ferrofluids. Microfluid Nanofluid. 2010;9:1003–9.
88. Subramaniam AB, Yang D, Yu HD, Nemiroski A, Tricard S, Ellerbee AK, et al. Noncontact orientation of objects in three-dimensional space using magnetic levitation. Proc Natl Acad Sci U S A. 2014;111:12980–5.
89. Mirica KA, Shevkoplyas SS, Phillips ST, Gupta M, Whitesides GM. Measuring densities of solids and liquids using magnetic levitation: fundamentals. J Am Chem Soc. 2009;131:10049–58.
90. Mirica KA, Phillips ST, Mace CR, Whitesides GM. Magnetic levitation in the analysis of foods and water. J Agric Food Chem. 2010;58:6565–9.
91. Guevorkian K, Valles JM Jr. Swimming Paramecium in magnetically simulated enhanced, reduced, and inverted gravity environments. Proc Natl Acad Sci U S A. 2006;103:13051–6.
92. Gao QH, Zhang WM, Zou HX, Li WB, Yan H, Peng ZK, et al. Label-free manipulation via the magneto-Archimedes effect: fundamentals, methodology and applications. Mater Horiz. 2019;6:1359–79.
93. Socoliuc V, Avdeev MV, Kuncser V, Turcu R, Tombácz E, Vékás L. Ferrofluids and bio-ferrofluids: looking back and stepping forward. Nanoscale. 2022;14:4786–886.
94. Shen F, Hwang H, Hahn YK, Park JK. Label-free cell separation using a tunable magnetophoretic repulsion force. Anal Chem. 2012;84:3075–81.

95. Nguyen NT. Micro-magnetofluidics: interactions between magnetism and fluid flow on the microscale. Microfluid Nanofluid. 2012;12:440.
96. Sekine W, Haraguchi Y, Shimizu T, Umezawa A, Okano T. Thickness limitation and cell viability of multi-layered cell sheets and overcoming the diffusion limit by a porous-membrane culture insert. J Biochips Tissue Chips. 2011;s1:007.
97. Ito A, Jitsunobu H, Kawabe Y, Kamihira M. Construction of heterotypic cell sheets by magnetic force-based 3-D coculture of HepG2 and NIH3T3 cells. J Biosci Bioeng. 2007;104:371–8.
98. Rouwkema J, Khademhosseini A. Vascularization and angiogenesis in tissue engineering: beyond creating static networks. Trends Biotechnol. 2016;34:733–45.
99. Amini AR, Laurencin CT, Nukavarapu SP. Bone tissue engineering: recent advances and challenges. Crit Rev Biomed Eng. 2012;40:363–408.
100. Silva AS, Santos LF, Mendes MC, Mano JF. Multi-layer prevascularized magnetic cell sheets for bone regeneration. Biomaterials. 2020;231:119664.
101. Lopes D, Martins-Cruz C, Oliveira MB, Mano JF. Bone physiology as inspiration for tissue regenerative therapies. Biomaterials. 2018;185:240–75.
102. Correia CR, Pirraco RP, Cerqueira MT, Marques AP, Reis RL, Mano JF. Semipermeable capsules wrapping a multifunctional and self-regulated co-culture microenvironment for osteogenic differentiation. Sci Rep. 2016;6:21883.
103. Moschouris K, Firoozi N, Kang Y. The application of cell sheet engineering in the vascularization of tissue regeneration. Regen Med. 2016;11:559–70.
104. Koto W, Shinohara Y, Kitamura K, Wachi T, Makihira S, Koyano K. Porcine dental epithelial cells differentiated in a cell sheet constructed by magnetic nanotechnology. Nanomaterials (Basel). 2017;7:322.
105. Thesleff I. Epithelial-mesenchymal signalling regulating tooth morphogenesis. J Cell Sci. 2003;116:1647–8.
106. Young CS, Terada S, Vacanti JP, Honda M, Bartlett JD, Yelick PC. Tissue engineering of complex tooth structures on biodegradable polymer scaffolds. J Dent Res. 2002;81:695–700.
107. Puthiyaveetil JS, Kota K, Chakkarayan R, Chakkarayan J, Thodiyil AK. Epithelial-mesenchymal interactions in tooth development and the significant role of growth factors and genes with emphasis on mesenchyme-a review. J Clin Diagn Res. 2016;10:ZE05–9.
108. Uskoković V. Amelogenin in enamel tissue engineering. Adv Exp Med Biol. 2015;881:237–54.
109. Nanci A, Zalzal S, Lavoie P, Kunikata M, Chen W, Krebsbach PH, et al. Comparative immunochemical analyses of the developmental expression and distribution of ameloblastin and amelogenin in rat incisors. J Histochem Cytochem. 1998;46:911–34.
110. Ravindranath HH, Chen LS, Zeichner-David M, Ishima R, Ravindranath RM. Interaction between the enamel matrix proteins amelogenin and ameloblastin. Biochem Biophys Res Commun. 2004;323:1075–83.
111. Fukumoto S, Kiba T, Hall B, Iehara N, Nakamura T, Longenecker G, et al. Ameloblastin is a cell adhesion molecule required for maintaining the differentiation state of ameloblasts. J Cell Biol. 2004;167:973–83.
112. Hatakeyama J, Fukumoto S, Nakamura T, Haruyama N, Suzuki S, Hatakeyama Y, et al. Synergistic roles of amelogenin and ameloblastin. J Dent Res. 2009;88:318–22.
113. Deutsch D, Palmon A, Fisher LW, Kolodny N, Termine JD, Young MF. Sequencing of bovine enamelin ("tuftelin") a novel acidic enamel protein. J Biol Chem. 1991;266:16021–8.
114. Hsiao AY, Torisawa YS, Tung YC, Sud S, Taichman RS, Pienta KJ, et al. Microfluidic system for formation of PC-3 prostate cancer co-culture spheroids. Biomaterials. 2009;30:3020–7.
115. Chan HF, Zhang Y, Ho YP, Chiu YL, Jung Y, Leong KW. Rapid formation of multicellular spheroids in double-emulsion droplets with controllable microenvironment. Sci Rep. 2013;3:3462.
116. Vadivelu RK, Kamble H, Shiddiky MJA, Nguyen NT. Microfluidic technology for the generation of cell spheroids and their applications. Micromachines (Basel). 2017;8:94.
117. Zhao Z, Gu J, Zhao Y, Guan Y, Zhu XX, Zhang Y. Hydrogel thin film with swelling-induced wrinkling patterns for high-throughput generation of multicellular spheroids. Biomacromol. 2014;15:3306–12.
118. Cheng NC, Wang S, Young TH. The influence of spheroid formation of human adipose-derived stem cells on chitosan films on stemness and differentiation capabilities. Biomaterials. 2012;33:1748–58.
119. Dzamukova MR, Naumenko EA, Lannik NI, Fakhrullin RF. Surface-modified magnetic human cells for scaffold-free tissue engineering. Biomater Sci. 2013;1:810–3.
120. Lin RZ, Chu WC, Chiang CC, Lai CH, Chang HY. Magnetic reconstruction of three-dimensional tissues from multicellular spheroids. Tissue Eng Part C Methods. 2008;14:197–205.
121. Olsen TR, Mattix B, Casco M, Herbst A, Williams C, Tarasidis A, et al. Manipulation of cellular spheroid composition and the effects on vascular tissue fusion. Acta Biomater. 2015;13:188–98.
122. Nath S, Devi GR. Three-dimensional culture systems in cancer research: focus on tumor spheroid model. Pharmacol Ther. 2016;163:94–108.
123. Ong CS, Zhou X, Han J, Huang CY, Nashed A, Khatri S, et al. In vivo therapeutic applications of cell spheroids. Biotechnol Adv. 2018;36:494–505.
124. Ivascu A, Kubbies M. Rapid generation of single-tumor spheroids for high-throughput cell function and toxicity analysis. J Biomol Screen. 2006;11:922–32.
125. Bratt-Leal AM, Kepple KL, Carpenedo RL, Cooke MT, McDevitt TC. Magnetic manipulation and spatial patterning of multi-cellular stem cell aggregates. Integr Biol. 2011;3:1224–32.
126. Jafari J, Han XL, Palmer J, Tran PA, O'Connor AJ. Remote control in formation of 3D multicellular assemblies using magnetic forces. ACS Biomater Sci Eng. 2019;5:2532–42.
127. Lewis NS, Lewis EE, Mullin M, Wheadon H, Dalby MJ, Berry CC. Magnetically levitated mesenchymal stem cell spheroids cultured with a collagen gel maintain phenotype and quiescence. J Tissue Eng. 2017;8:2041731417704428.
128. Bonab MM, Alimoghaddam K, Talebian F, Ghaffari SH, Ghavamzadeh A, Nikbin B. Aging of mesenchymal stem cell in vitro. BMC Cell Biol. 2006;7:14.
129. Banfi A, Muraglia A, Dozin B, Mastrogiacomo M, Cancedda R, Quarto R. Proliferation kinetics and differentiation potential of ex vivo expanded human bone marrow stromal cells: Implications for their use in cell therapy. Exp Hematol. 2000;28:707–15.
130. Lin SP, Chiu FY, Wang Y, Yen ML, Kao SY, Hung SC. RB maintains quiescence and prevents premature senescence through upregulation of DNMT1 in mesenchymal stromal cells. Stem Cell Rep. 2014;3:975–86.
131. Engler AJ, Sen S, Sweeney HL, Discher DE. Matrix elasticity directs stem cell lineage specification. Cell. 2006;126:677–89.
132. Nilsson SK, Debatis ME, Dooner MS, Madri JA, Quesenberry PJ, Becker PS. Immunofluorescence characterization of key extracellular matrix proteins in murine bone marrow in situ. J Histochem Cytochem. 1998;46:371–7.

133. Kolf CM, Cho E, Tuan RS. Mesenchymal stromal cells. Biology of adult mesenchymal stem cells: regulation of niche, self-renewal and differentiation. Arthritis Res Ther. 2007;9:204.
134. Méndez-Ferrer S, Michurina TV, Ferraro F, Mazloom AR, Macarthur BD, Lira SA, et al. Mesenchymal and haematopoietic stem cells form a unique bone marrow niche. Nature. 2010;466:829–34.
135. Tzeng YS, Li H, Kang YL, Chen WC, Cheng WC, Lai DM. Loss of Cxcl12/Sdf-1 in adult mice decreases the quiescent state of hematopoietic stem/progenitor cells and alters the pattern of hematopoietic regeneration after myelosuppression. Blood. 2011;117:429–39.
136. Anil-Inevi M, Yaman S, Yildiz AA, Mese G, Yalcin-Ozuysal O, Tekin HC, et al. Biofabrication of in situ self assembled 3D cell cultures in a weightlessness environment generated using magnetic levitation. Sci Rep. 2018;8:7239.
137. Haisler WL, Timm DM, Gage JA, Tseng H, Killian TC, Souza GR. Three-dimensional cell culturing by magnetic levitation. Nat Protoc. 2013;8:1940–9.
138. Tasoglu S, Khoory JA, Tekin HC, Thomas C, Karnoub AE, Ghiran IC, et al. Levitational image cytometry with temporal resolution. Adv Mater. 2015;27:3901–8.
139. Durmus NG, Tekin HC, Guven S, Sridhar K, Arslan Yildiz A, Calibasi G, et al. Magnetic levitation of single cells. Proc Natl Acad Sci U S A. 2015;112:E3661–8.
140. Greco G, Agostini M, Tonazzini I, Sallemi D, Barone S, Cecchini M. Surface-acoustic-wave (SAW)-driven device for dynamic cell cultures. Anal Chem. 2018;90:7450–7.
141. Ha BH, Lee KS, Destgeer G, Park J, Choung JS, Jung JH, et al. Acoustothermal heating of polydimethylsiloxane microfluidic system. Sci Rep. 2015;5:11851.
142. Shilton RJ, Mattoli V, Travagliati M, Agostini M, Desii A, Beltram F, et al. Rapid and controllable digital microfluidic heating by surface acoustic waves. Adv Funct Mater. 2015;25:5895–901.
143. Park J, Jung JH, Destgeer G, Ahmed H, Park K, Sung HJ. Acoustothermal tweezer for droplet sorting in a disposable microfluidic chip. Lab Chip. 2017;17:1031–40.
144. Park J, Ha BH, Destgeer G, Jung JH, Sung HJ. Spatiotemporally controllable acoustothermal heating and its application to disposable thermochromic displays. RSC Adv. 2016;6:33937–44.
145. Ha BH, Park J, Destgeer G, Jung JH, Sung HJ. Generation of dynamic free-form temperature gradients in a disposable microchip. Anal Chem. 2015;87:11568–74.
146. Thevenard L, Camara IS, Prieur J-Y, Rovillain P, Lemaître A, Gourdon C, et al. Strong reduction of the coercivity by a surface acoustic wave in an out-of-plane magnetized epilayer. Phys Rev B. 2016;93:140405.
147. Wiklund M. Acoustofluidics 12: biocompatibility and cell viability in microfluidic acoustic resonators. Lab Chip. 2012;12:2018–28.
148. Lam KH, Li Y, Li Y, Lim HG, Zhou Q, Shung KK. Multifunctional single beam acoustic tweezer for non-invasive cell/organism manipulation and tissue imaging. Sci Rep. 2016;6:37554.
149. Pan Y, Du X, Zhao F, Xu B. Magnetic nanoparticles for the manipulation of proteins and cells. Chem Soc Rev. 2012;41:2912–42.
150. Ashkarran AA, Mahmoudi M. Magnetic levitation systems for disease diagnostics. Trends Biotechnol. 2021;39:311–21.
151. Munaz A, Shiddiky MJA, Nguyen NT. Recent advances and current challenges in magnetophoresis based micro magnetofluidics. Biomicrofluidics. 2018;12:031501.
152. Rufo J, Zhang P, Zhong R, Lee LP, Huang TJ. A sound approach to advancing healthcare systems: the future of biomedical acoustics. Nat Commun. 2022;13:3459.
153. Ma Z, Holle AW, Melde K, Qiu T, Poeppel K, Kadiri VM, et al. Acoustic holographic cell patterning in a biocompatible hydrogel. Adv Mater. 2020;32:e1904181.
154. Gu Y, Chen C, Rufo J, Shen C, Wang Z, Huang PH, et al. Acoustofluidic holography for micro- to nanoscale particle manipulation. ACS Nano. 2020;14:14635–45.
155. Baudoin M, Thomas JL, Sahely RA, Gerbedoen JC, Gong Z, Sivery A, et al. Spatially selective manipulation of cells with single-beam acoustical tweezers. Nat Commun. 2020;11:4244.
156. Betsch M, Cristian C, Lin YY, Blaeser A, Schöneberg J, Vogt M, et al. Incorporating 4D into bioprinting: real-time magnetically directed collagen fiber alignment for generating complex multilayered tissues. Adv Healthc Mater. 2018;7:e1800894.
157. Etoc F, Lisse D, Bellaiche Y, Piehler J, Coppey M, Dahan M. Subcellular control of Rac-GTPase signalling by magnetogenetic manipulation inside living cells. Nat Nanotechnol. 2013;8:193–8.
158. Stanley SA, Sauer J, Kane RS, Dordick JS, Friedman JM. Remote regulation of glucose homeostasis in mice using genetically encoded nanoparticles. Nat Med. 2015;21:92–8.
159. Liße D, Monzel C, Vicario C, Manzi J, Maurin I, Coppey M, et al. Engineered ferritin for magnetogenetic manipulation of proteins and organelles inside living cells. Adv Mater. 2017;29:1700189.
160. Armstrong JPK, Stevens MM. Using remote fields for complex tissue engineering. Trends Biotechnol. 2020;38:254–63.